NPS-61-89-001

NAVAL POSTGRADUATE SCHOOL

Monterey, California

LASER ALTIMETER FOR USE OVER THE OCEAN

E. C. Crittenden, Jr., G. W. Rodeback
A. W. Cooper, and C. M. Bourne

April, 1989

Final Report

for Period October 1987-September 1988

Approved for public release; distribution unlimited.

r:
ystems Command
6W31
DC 20362-5101

NAVAL POSTGRADUATE SCHOOL

Rear Admiral R.C. Austin
Superintendent

Dean H. Schull
Provost

The work reported herein was supported by

Naval Sea Systems Command Sea 06 W21 under documents N0002487WR10830 and N0002487AFE84YX

This report was prepared by:

CURITY CLASSIFICATION OF THIS PAGE

REPORT DOCUMENTATION PAGE

1a. REPORT SECURITY CLASSIFICATION UNCLASSIFIED	1b. RESTRICTIVE MARKINGS
2a. SECURITY CLASSIFICATION AUTHORITY	3. DISTRIBUTION/AVAILABILITY OF REPORT Approved for public release; distribution unlimited
2b. DECLASSIFICATION/DOWNGRADING SCHEDULE	
4. PERFORMING ORGANIZATION REPORT NUMBER(S) NPS61-89-001	5. MONITORING ORGANIZATION REPORT NUMBER(S)
6a. NAME OF PERFORMING ORGANIZATION AVAL POSTGRADUATE SCHOOL 6b. OFFICE SYMBOL (If applicable) Dept 61	7a. NAME OF MONITORING ORGANIZATION
6c. ADDRESS (City, State, and ZIP Code) Monterey, California 93943-5000	7b. ADDRESS (City, State, and ZIP Code)
8a. NAME OF FUNDING/SPONSORING ORGANIZATION Naval Sea Systems Command 8b. OFFICE SYMBOL (If applicable) SEA 06 W31	9. PROCUREMENT INSTRUMENT IDENTIFICATION NUMBER N0002487WR10830 N0002487AFE84YX
8c. ADDRESS (City, State, and ZIP Code) Washington, DC 20362-5101	10. SOURCE OF FUNDING NUMBERS PROGRAM ELEMENT NO. / PROJECT NO. / TASK NO. / WORK UNIT ACCESSION NO.

11. TITLE (Include Security Classification)
LASER ALTIMETER FOR USE OVER THE OCEAN (U)

12. PERSONAL AUTHOR(S)
E. C. Crittenden, Jr., G. W. Rodeback, A. W. Cooper and C. M. Bourne

13a. TYPE OF REPORT	13b. TIME COVERED	14. DATE OF REPORT (Year, Month, Day)	15. PAGE COUNT
Interim	FROM 1987 TO 1988	1989 April	77

16. SUPPLEMENTARY NOTATION

17. COSATI CODES			18. SUBJECT TERMS (Continue on reverse if necessary and identify by block number)
FIELD	GROUP	SUB-GROUP	Laser Altimeter, Reflectance and Sea State, Sea Surface Reflectance

19. ABSTRACT (Continue on reverse if necessary and identify by block number)

A pilot model of a small size, mass, power, and cost, GaAs laser radar altimeter has been developed and tested for use over the ocean. Two versions have been developed, one for triggering a device at a predetermined altitude, and one for providing an altitude "read-out" as an analog dc voltage. Field tests from a bridge over an inland reservoir indicate performance with negligible false-alarm rate up to an altitude of 400 meters over the ocean, under all sea-state conditions, from glassy calm to the "worst-case" rough sea state condition, and with the sun vertically overhead. A new remote sensing technique was developed to evaluate the roughness state of the water during field tests and to predict the mean laser return signal. This utilizes video imaging of the glitter pattern on the water from a bright point source light at night, or from the sun in the daytime. Tests of the altimeter over the ocean surface at sea are still needed, because extrapolation from riddles on the inland reservoir to full scale ocean waves is not fully understood.

20. DISTRIBUTION/AVAILABILITY OF ABSTRACT ☒ UNCLASSIFIED/UNLIMITED ☐ SAME AS RPT. ☐ DTIC USERS	21. ABSTRACT SECURITY CLASSIFICATION UNCLASSIFIED
22a. NAME OF RESPONSIBLE INDIVIDUAL A. W. Cooper	22b TELEPHONE (Include Area Code) (408) 646-2452 22c OFFICE SYMBOL 61Cr

D FORM 1473, 84 MAR 83 APR edition may be used until exhausted.
All other editions are obsolete

SECURITY CLASSIFICATION OF THIS PAGE

☆ U.S. Government Printing Office: 1986—606-24

SUMMARY

A pilot model of a laser radar altimeter has been developed and tested. The altimeter is intended for use in parachute-suspended off-board devices deployed over the ocean from deck-mounted mortar launchers. The model meets the requirements of small size, small mass, low power, small cost, and inherent resistance to high acceleration loading. The laser transmitter is a 0.905 nanometer, 5 element, GaAs pulsed laser array, rated at 75 watts peak power. The detector for the returned signal is a silicon avalanche photodiode.

Field tests of the model have been made from a bridge over an inland reservoir at a vertical range of 45 meters. The tests indicate that this model will perform satisfactorily at vertical ranges up to 400 meters over the ocean, under all sea-state conditions, from glassy calm to the "worst-case" rough sea state condition, and with the sun vertically overhead.

A new remote sensing technique was developed and utilized to evaluate the roughness state of the water at the time of laser return signal measurement. This system utilizes video imaging of the glitter pattern reflected from the water surface when it is illuminated by a bright point source light at night, or by the sun in the daytime. A tentative theoretical model allows estimation of the magnitude of the mean laser return signal for the worst case of extremely rough water. Tests of the system at full altitude over a real ocean surface are still needed, and are planned, because extrapolation from ripples on the inland reservoir to full scale waves is not fully understood.

The false alarm rate is almost entirely determined by the shot noise due to reflection of sunlight. The false alarm rate is reduced to negligible level by inclusion of a narrow time window for the returned signals, use of a double pulse return requirement, and inclusion of a gain control system to limit the amplifier gain for large solar reflection glints. Measurements of solar noise were made with the sun as near vertical as possible (14 degrees from vertical) at the latitude of central California. With noise extrapolated to the case of an overhead sun, the measured false alarm rate is one in 80,000 parachute descents of 60 seconds duration.

For quite different application, a modification of the receiver electronic circuits was also developed which permits the same laser altimeter hardware to provide a "read-out" in the form of an analog voltage that is proportional to the altitude.

TABLE OF CONTENTS

(Continued, next page)

LIST OF FIGURES

LIST OF TABLES

I. INTRODUCTION

Several types of altimeters have been used for the activation of mortar launched devices. Activation is desired at a preset distance above the ocean surface while the device descends on a parachute. Both aneroid altimeters and radar altimeters have been used but suffer from lack of reliability. Also, the radar altimeters tended to be too expensive and bulky. The altimeter has to be able to function at altitudes up to 150 meters and be small enough and light enough to permit incorporating within a round to be fired from a deck-mounted mortar launcher. It also has to withstand the acceleration encountered during such launching. As it is to be expendable, the altimeter has to be inexpensive. It seemed feasible to meet these requirements with a laser radar altimeter utilizing a gallium arsenide semiconductor diode laser, with the return signal detected with a silicon avalanche photodiode. Additionally, in the course of this work, a Navy interest developed in utilizing the same system to provide an altitude "read-out" for other applications. The two objectives have much in common. This report summarizes the work done to achieve both a "triggering" laser altimeter for activation of a countermeasure at a preset altitude above the ocean and an altitude read-out laser altimeter.

II. OPTIMUM LASER ALTIMETER DESIGN

1. Laser

The weight, volume, and cost limit the possible laser type to the pulsed semiconductor diode laser, with gallium arsenide as the most available and the least expensive at $20 to $200 per laser, for 20 to 100 watts peak optical power output. The transmitted radiation from these lasers is at a wavelength of 0.905 micrometers. This wavelength is well matched to silicon diode photodetectors for the receiver. The pulse length usually employed for gallium arsenide junction lasers is about 150 nsec at half height. The pulses are easily generated. This short pulse length does not seriously limit the gain of the high gain receiver electronics because only the leading edge of the pulse is needed to trigger the range gate. If the full pulse shape were needed, the limitation would be severe. Pulse repetition rates up to about 3 kHz are possible for these diode lasers. Rates of about 1 kHz were used in this application.

2. Triggering

The response of the altitude determining circuit is triggered when the time delay of a received pulse is less than 1.0 microsecond, the round trip time for the laser pulse at an altitude of 150 meters. The altitude for triggering can be adjusted by changing the triggering time delay. The trigger circuitry is so arranged that the system can respond only to pulses that are larger than a preset threshold voltage. For the altitude "triggering" device, for which the false alarm rate is critical, the circuit responds only to pulses received within a narrow time window surrounding the expec-

ted time of arrival of a return pulse at the preset altitude. This sharply reduces the probability of accidental triggering on noise. Quantitative data on the false alarm rate is given in section VI.

For the altitude read-out device, the time window needs to be longer in order to include pulses returning from any range over which the device is expected to operate. This permits a larger number of false triggerings. However, the false alarm rate is not a critical problem for the readout device, since it is steadily triggered, and the average reading is only slightly modified by an occasional false trigger. Sunlight noise is also a smaller problem, since the operator can presumably elect to make the measurement at a time when the sun is not directly overhead.

For both the triggering and the readout device, the probability of a false alarm trigger due to noise from sunlight is reduced by requiring two sequential triggerings. This has been done in both devices, as will be reported in section III and section V.

3. Laser Transmitter Beam Pattern.

Reflection from a rough water surface takes the form of a "glitter" pattern that is approximately elliptical in shape and with a nearly Gaussian profile. In detail the profile is Gram-Charlier, to be discussed later in section IV of this report. The size of the major and minor axes of the elliptical glitter pattern are dependent on sea state. The returned signal is maximum if the transmitted beam and the acceptance cone of the receiver are collinear and the receiver cone solid angle is larger than the transmitter cone. The returned signal is also maximized if the transmitter and receiver cone angles are vertical and are small compared to the glitter pattern "width". These considerations dictate small transmitter and receiver cone angles.

Swinging of the descending parachute-supported package could lead to failure to trigger the device, if the sea were flat calm and a very small cone angle utilized. In a calm but "lumpy" sea a narrow beam could similarly fail to trigger. An offset fan shaped beam pattern, with one end of the flat fan on the vertical, could minimize this possibility, but the system then suffers some in sensitivity due to increased beam solid angle. A practical problem is that long narrow detectors are not at present available in avalanche photodiodes. A linear array, with signals added electronically, would be a later development with some merit. Such arrays are not yet available in inexpensive avalanche detectors.

In view of the above considerations a small solid angle beam pattern with circular cross-section about one degree was used in the experi ments to be reported later in this report.

4. Laser Transmitter Optics

At first sight, plastic Fresnel lenses would seem to be ideal for this application as they have low mass, require small space, have large aperture (aspheric), are inexpensive, and could be molded into the aerodynamic dome. Unfortunately, the scattering at the facets in the face of these lenses is too large to tolerate because the consequent resolution is too poor to adequately define the beam. As a result achromatically corrected cemented-pair glass lenses were used. The achromatism is not needed because the laser radiation is quite monochromatic. The important feature is that such lenses are also corrected for coma and astigmatism. They are also relatively inexpensive. In the design used in the experiments to be reported here, the beam forming lens was a 2.5 inch focal length, 1.5 inch diameter, achromatic lens.

5. Receiver photodetector choice

Although photomultipliers have high gain and good signal-to-noise ratio, they are impractical for this application because of large size and fragile glass envelope which would be unable to withstand the high g loading of deployment in a mortar fired round. They also usually require a very well regulated high voltage power supply (1000 v.).

In contrast to photomultipliers, silicon semiconductor junction photodiodes are rugged against high g loading, occupy a very small volume (1/4 inch cube), have their peak responsivity near 0.905 micrometers, and require relatively low voltage (90 volts). They are also inexpensive ($10), are available from many suppliers and with some variability in geometry. However they are limited to a maximum responsivity of about 0.5 amps/watt, inadequate for the signal-to-noise ratio requirements of this application.

The silicon avalanche photodiode, an evolution from the photodiode, has most of the advantages of the photodiode except for some increase in price. These detectors have previously been quite high priced, but the prices have dropped sharply recently, with some types now available at $50-100. The avalanche photodiode has a crucial improvement over the photodiode in that the signal-to-noise ratio can be increased relative to the photodiode by about a factor of 30. This factor changes the performance in this application from marginally practical to clearly practical. The capacitance is also smaller than that of the photodiode, providing increased pulse responsivity.

The internal gain of avalanche photodiodes increases rapidly with increasing applied voltage above the avalanche threshold. Although this requires good power supply voltage regulation, it provides a simple mechanism for varying the gain of the system as a function of the magnitude of sunlight induced photocurrent. When the sea surface is such as to produce a large laser reflectance, it also produces a large sunlight reflectance, and consequent shot noise. However the solar glints are slow compared to the

laser pulses, so the gain can be automatically reduced by the slow IR drop produced by the solar current. This permits automatic adjustment to match variations in sea surface reflectance. This is discussed in detail in sections V, VI, and VII.

In view of these considerations, the clearly superior detector for this application is the silicon avalanche photodiode.

6. Avalanche Photodiode Signal

The maximum pulse responsivity is achieved if the avalanche photodiode is used as a charge collector, that is, with a high load resistor. The received signal peak magnitude is approximately q/C (charge collected/capacitance of the photocell, the input FET follower, and the connecting lead). The peak of the pulse signal is slightly reduced by the RC decay occurring during the rise time. The signal is thus essentially proportional to the time-integral of the received light flux power. With a laser pulse length of 180 nanoseconds, measured at half height, the response reaches half height in about 50 nanoseconds. The pulse amplifier reaches half height in about 75 nanoseconds with a slower recovery. There is no penalty on slow amplifier recovery, as long as it occurs within the time interval between successive pulses (one millisecond).

Sunlight reflected from the water surface can produce a large slowly varying photocurrent. The characteristic time for the variation of this current is in milliseconds. This current produces shot noise and is the dominant noise of concern in the system. Its magnitude is reduced as far as possible by an optical bandpass filter placed in front of the receiver optics. The bandwidth of the optical filter must be large enough to pass the spread in wavelength of the laser. This width is mostly due to longitudinal modes in the diode laser. A 5 nanometer bandwidth filter could be used as the minimum, except that such filters are expensive. 10 nanometer bandwidth filters are available from suppliers at about $50 as off-the-shelf items. Even an off-the-shelf filter is thus one of the major cost items in the system.

The slowly varying solar signal is blocked from the pulse signal preamplifier by means of a high-pass electrical filter at the preamplifier input. This electrical filter prevents the low frequency sun glint from triggering the device but does not reduce the shot noise generated by the current due to sunlight. Several systems are utilized in the altimeter circuits to minimize the effects of this shot noise. These systems are discussed in detail in sections V, VI, and VII.

7. Receiver Optical System

In the optical design, reduction of the acceptance solid angle of the receiver, and increase in the diameter of the input aperture, increase the signal-to-noise ratio, provided that the emitter pattern solid angle lies

within the receiver solid angle. The present design uses approximately a one degree circular cone. As mentioned above, the possibility of swinging of the descending countermeasure package indicates that a better design would incorporate a fan-shaped cone, to increase the probability of passing through vertical orientation for near calm sea states. However, the required detector geometry is not available in avalanche photodetectors at present.

8. Optical Design Optimization

Optimization of the optical design is somewhat forced by the availability of avalanche photodiodes that are inexpensive and have high gain. In particular, the sensitive areas available all lie very close to 0.5 mm diameter. In addition, the capacitance of the detector is so small that the capacitance of the connecting lead and input to the FET follower are comparable to that of the detector. This means that the detector size and capacitance is fixed.

To optimize the signal-to-noise ratio, where the noise is due to the sunlight reflected from the surface, requires determining the solar flux collected.

Solar noise

Taking the surface reflection to be Lambertian, the solar power on the detector is

$$P = F\ A_t\ A_l / Z^2$$

Where F is the reflected flux per unit solid angle
A_t is the reflecting area seen by the detector
A_l is the area of the lens
and Z is the distance of the lens from the reflecting surface

The reflecting area seen by the detector is given by

$$A_t = S_d\ Z^2$$

Where S_d is the solid angle subtended by the detector at the lens and Z is the range (distance of the system from the water).

Substituting:

$$P = F_s\ S_d\ Z^2\ A_l / Z^2$$

and canceling Z^2

$$P = F_s\ S_d\ A_l$$

Now $S_d = A_d/L^2$

Where A_d is the area of the detector

Substituting

$$P = F_s A_d A_l / L^2$$

The current flowing is then

$$I_s = P R = F_s A_d A_l R /L^2$$

Where R is the detector responsivity, or current/power.

The RMS noise voltage, N, is proportional to the square root of the current, so

$$N \approx \sqrt{I_s} = \sqrt{F_s A_d A_l R /L^2}$$

But, since F_s and A_d are constants,

$$N \approx \sqrt{A_l R /L^2}$$

Pulse Response

Provided that the laser spot falls entirely within the water surface area seen by the detector, then the energy received by the detector due to a laser return pulse is given by

$$E = F_l A_l / Z^2$$

Where F_l is the flux per unit solid angle returned from the surface as the result of laser illumination.

The charge, q, passed by the detector is then given by

$$q = E R$$

or $$q = F_l A_l R /Z^2$$

Now $V = q/C$

Where C is the capacitance of the detector and follower input

Substituting yields

$$V = F_l A_l R /CZ^2$$

Now the signal-to-noise ratio is given by

$$V/N \approx \frac{F_1 A_1 R / CZ^2}{\sqrt{F_s A_d A_1 R / L^2}}$$

But, because F_1, C, F_s, and A_d are all constants, they can be omitted.

Thus $V/N \approx L \sqrt{A_1 R}$

and, since $D \approx \sqrt{A_1}$

$$V/N \approx D L \sqrt{R}$$

Thus the signal-to-noise ratio depends on the product of the lens diameter, D, the focal length, L, and the square root of the Responsivity, R.

The present design utilizes receiver optics with a focal length of 27 mm and diameter 16 mm. The lens is an "achromatic" lens, not because of the color correction, but because such lenses are also corrected for coma and spherical aberration. The present cone of acceptance of the receiver has a divergence of 1.1 degrees. The laser transmitter is adjusted so that the transmitted beam lies within this cone

Components have been purchased for an alternative optical system with a 35 mm focal length and 23 mm diameter. This system should provide a signal-to-noise improvement over the present system by a factor

$$(23/16)(35/27) = 1.86$$

The signal, proportional to A_1, should increase in the ratio

$$35^2/16^2 = 4.78$$

This alternative system has not been tested as yet.

9. LASER ALTIMETER PARAMETERS, AND PRICING

After early tests on a sequence of five preliminary test models, a sixth pilot model was constructed to optimize the design for use in field tests in which the roughness state of the water was determined by companion measurements of the glitter pattern with a video camera. The choices made in this design were based on the considerations discussed in the preceding section of this report. The laser altimeter design is summarized below.

TABLE 1. LASER ALTIMETER PARAMETERS

Laser:	
LD167, from Laser Diode Labs of the M/A COM corporation,	$208
Emission area: Five parallel .030 inch long lines, pattern 0.045 inch wide perpendicular to lines	
Power output: Approximately 75 watts peak	
Pulse length: 180 nanosec. at half height	
Power supply and voltage regulator: 80 volts;	$50
Primary pulse power: 2 Lithium batteries	$15
Pulse circuit: Assembled from small components; parts	$50
Transmitter optics:	
Lens: f/1.3 achromatic glass lens, 1.5 in. diameter, 2 in. focal length (Antireflection coated for visible; undesirable, but lenses available; transmission at 0.905 micrometers is 87%)	$15
Minimum spot size 0.5 by 0.8 degrees	
Defocussed to spot size 0.7 by 1.1 degrees	
Receiver Optics:	
Lens: Achromatic corrected glass lens, 27 mm focal length, 16 mm diameter, uncoated	$15
Filter: 905 nanometers, 10 nanometers bandwidth Corion Corp. SD10-905A	$50
Detector: Silicon avalanche photodiode; RCA type C30902E	$68
Sensitive area diameter: 0.5 mm	
Detector voltage supply, 100 to 300 volts	$60
Acceptance cone angle: 0.5/27 -> 1.1 degrees, circular	
Amplifier: Components	$30
Power supply: 4, 9 volt batteries	$6
Total	$567

The prices quoted above are single item prices as paid for the items utilized in the laser altimeter. Considerable reduction should apply for purchase in larger quantity.

III. ELECTRONIC SYSTEM

The circuits used in the "triggering" laser altimeter are closely related to those developed for the "readout" laser altimeter. Complete details of the circuits are presented in section VII of this report.

1. Circuit Functions

Shot noise fluctuation in the photodetector current due to reflected sunlight proves to be a dominant design problem. Although, as mentioned in section 1 of this report, the solar photocurrent is reduced by use of a narrow bandwidth optical filter, a number of additional techniques are needed to reduce the false alarm rate to an acceptable value. The behavior of the circuits used, and the specialized treatment to reduce the effects of sunlight noise, are described functionally below.

(1) The trigger circuit is constructed so that the derivative of the signal is the actual trigger. This provides a sharper time definition for the timing circuit than direct use of the return pulse signal.

(2) The response of the receiver amplifier is gated so that pulses are accepted only if they fall within a narrow time window located at the preset expected arrival time of the return laser pulse. Noise at any other time, until the next outgoing laser pulse one millisecond later, cannot trigger the system. This window is normally set at 100 nanoseconds width. Variation of this width allows a controlled change in the false alarm rate and permits direct measurement of the false alarm rate with data taken at rates that can be measured in a reasonable length of time. (In the "readout" laser altimeter this window is wider to permit the system to respond to whatever time delay is associated with the altitude being measured.)

(3) The system is so constructed that a triggering is not initiated unless two consecutive pulses meet all the other criteria. This feature reduces the triggering rate at the design trigger level by about a factor of 10^4 relative to single pulse triggering. Requiring a larger number of consecutive pulses would further reduce the false alarm rate but would begin to cause loss of legitimate return pulses, because the duration of glints from the water surface is of the order of a few milliseconds in the case of a fairly calm sea surface.

(4) The noise is minimized by limiting the bandwidth of the preamplifier input circuit to the minimum adequate to handle the laser return pulses.

2. Gain Control for Solar noise

For the "worst-case" sea state, the solar reflection signal and the laser return signal are both at their smallest values. As reported later in this

report, for this condition the signal-to-noise ratio is adequate to provide an acceptably small false alarm rate.

As the sea state becomes calmer than the "worst case", the laser return signal and the solar reflection current increase proportionally. Since the shot noise is proportional to the square root of the solar reflection current, the signal-to-noise ratio increases. However both signals are increasing in magnitude, so the false alarm rate due to noise triggering would increase unless the gain is reduced.

A system has been incorporated in the circuits so that an increase in the quasi-steady solar photocurrent decreases the voltage applied to the avalanche detector and thus decreases its gain. This provides a maximum limit to the solar produced noise. This noise limit was set slightly above the noise for solar reflection with the sun directly overhead and the worst-case rough sea state. The response speed of this control has purposely been made slow so that it regulates on the basis of the relatively slowly rising and falling sunlight glints in the millisecond range, and not in response to the laser return pulses, with about 90 nanosecond risetime. This time separation needs verification with real ocean waves, and is planned for later work.

The circuit diagram of the amplifier system is shown in Figure 1. The input end of this circuit, at the top of Figure 1, is shown in Figure 2. The amplitude of the fast-pulse laser return signals is primarily determined by the combined capacitance, C, of the avalanche detector plus the connecting leads, the dropping resistor R_1, and the input capacitance of the FET follower, F_1. The pulse signal is essentially q/C , where q is the charge generated in the avalanche photodiode in response to a laser pulse return from the water surface. The dropping resistor, R_1, determines the recovery time R_1C. This time can be allowed to be fairly long because the pulse timing is done with the leading edge of the pulses. The limit on recovery time is only that the system be fully recovered in time for the next pulse one millisecond later. This recovery time also determines the bandwidth for solar current shot noise. Increasing R_1 narrows the noise bandwidth, but increases the signal for slowly varying signals. The optimum value for this resistor appeared to be about 200k. This resistor also produces some inverse feedback to limit the noise current. A dc or low frequency current produces a drop in this resistor which lowers the potential applied to the avalanche detector. This reduction in potential then lowers the internal gain in the avalanche photodiode. In order to provide a much lower frequency inverse feedback, and time-average over the fast noise spikes, an additional 122k resistor, R_2, was inserted, together with the 0.1 microfarad capacitor between point A and ground. This filter does not affect the high frequency pulse signals, but limits the gain for sunlight glint signals in the millisecond range. This combination provides a limit to the solar generated shot noise at about 0.420 volts as measured at the output of the preamplifier.

Measurement of the false alarm rate under simulated sunlight noise is reported in section V of this report. Verification of the details of behavior over a real ocean surface and possible refinement of designs is planned for future work.

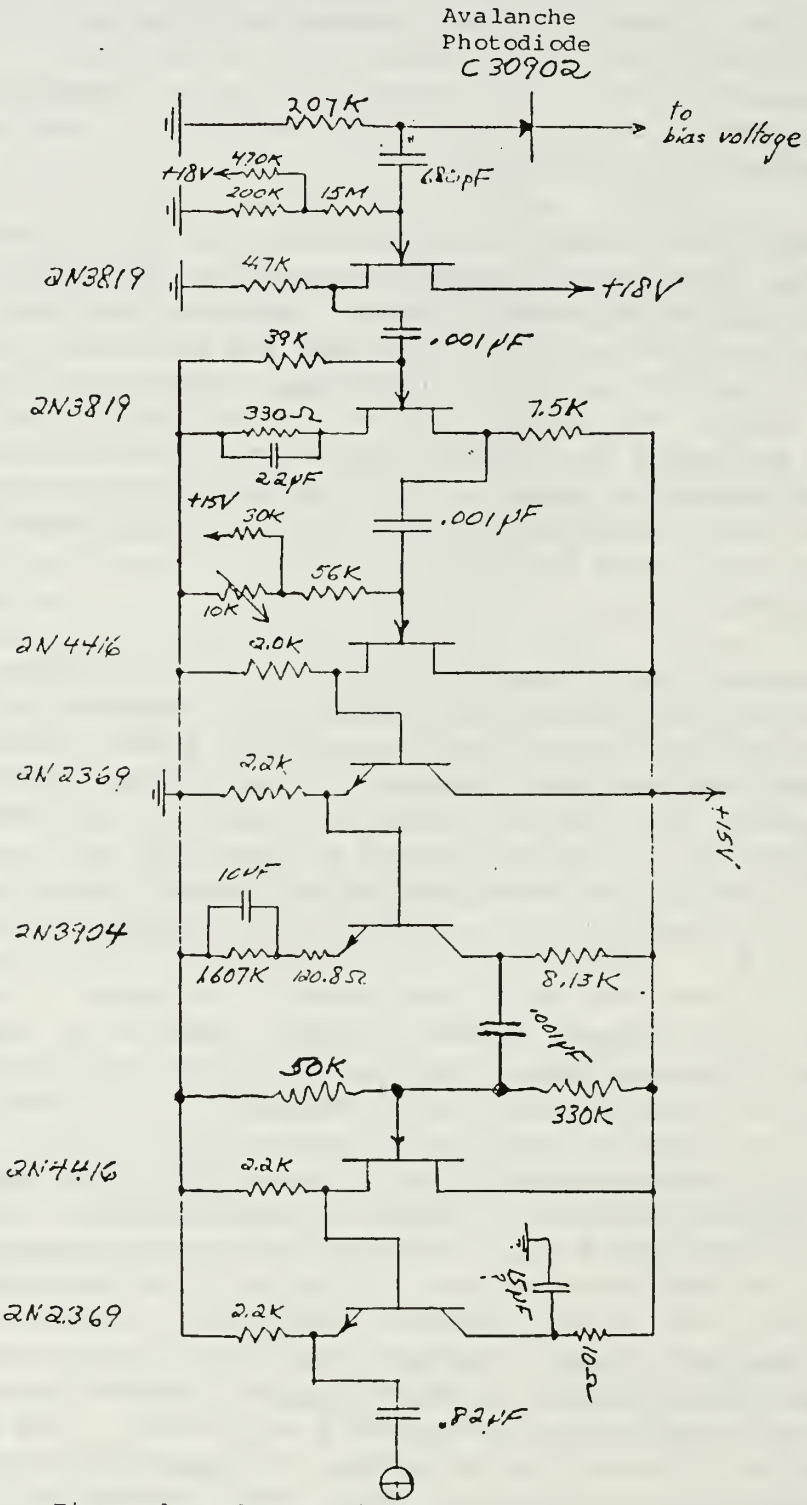

Figure 1. Pulse amplifier circuit

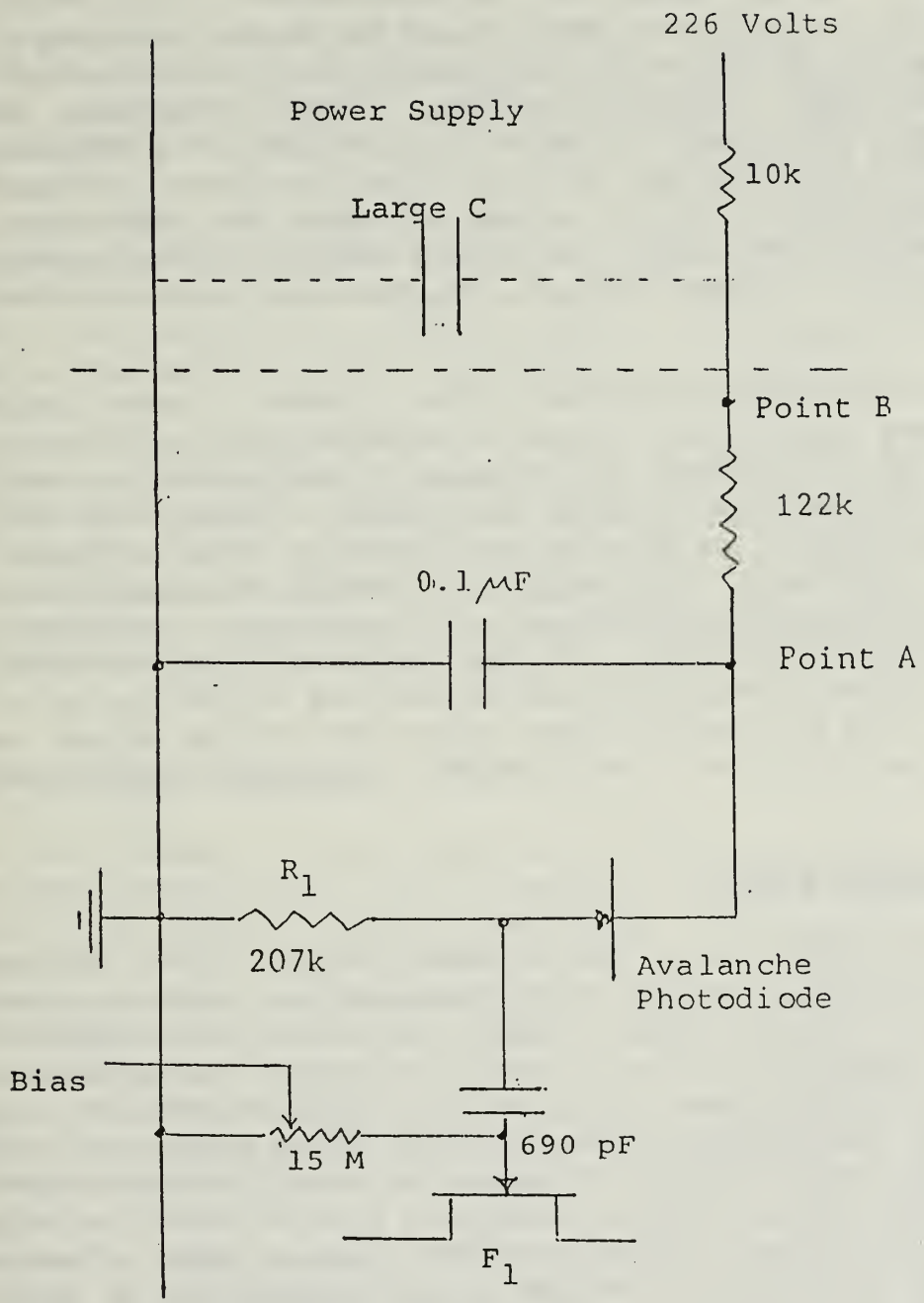

Figure 2. Circuit for gain regulation on the Avalanche Photodiode

IV. REMOTE SEA-STATE MEASUREMENT AND LASER RETURN SIGNAL

Determination and optimization of the performance of the various early models of the laser altimeter were carried out in the laboratory with measurements of the reflection from large plate glass windows, and from flat white, "Lambertian" reflecting surfaces. These measurements were also augmented with measurements of the reflected signal from a water surface as observed from a high bridge over an inland reservoir. Although these latter measurements gave some information about the performance of the laser altimeter it was largely qualitative because it had not been possible to evaluate the roughness state of the water surface at the instant of measurement.

With the present state of evolution of the altimeter it seemed desirable to carry out some experiments in which the roughness state could be evaluated. Prediction of the roughness on the basis of wind velocity seemed like a poor method as the sites available were subject to large local wind variations and the effects of previous wind velocity seemed difficult if not impossible to evaluate. Additionally a method of evaluating the roughness was needed that could be extended to use from aircraft. In effect a remote sensing technique was needed. In order to provide this capability, a new method of roughness measurement was devised and carried out in a set of experiments from the Parrotts Ferry bridge over the New Melones reservoir near Columbia California. The instruments were located 109 ft. above the water.

1. Remote Sensing Method

Papers in the literature by Cox and Munk[1], and by Petri[2], addressed the nature of the glitter pattern on the surface of the ocean in terms of the wind velocity. The information in these two papers taken together suggested that it might be possible to predict an expected laser radar return on the basis of a measurement of the width of glitter patterns. It also seemed likely that glitter patterns measured with a nearly point source of light at night would be simpler to obtain and would yield more directly the desired result than would glitter patterns obtained with the oblique illumination from the sun that had been used by Cox and Munk. Consequently, it seemed desirable to test the feasibility of prediction of laser return from the profile widths of glitter patterns obtained with a point light source. The tests indicated that laser return was related to glitter pattern width. In order to get a more specific relationship, a tentative theoretical model was developed. This has not as yet succeeded in predicting the absolute magnitude of laser return, but it does provide a functional relationship which is useful. The model predicts the ratio of laser radar return from the rough surface to that from an ideal Lambertian surface in terms of the glitter pattern width. Such a Lambertian surface is one which reflects equally in all directions for a surface of infinite extent. For a finite area, the reflectance of such a surface varies as the cosine of the angle from the normal, i.e. proportional to the projected

area. The Lambertian reflectance used for the water surface was also taken to have an overall reflectance equal to the specular reflectance coefficient for water of 0.0204 .

Glitter patterns from wind-driven water surface roughness have a Gram-Charlier distribution of light intensity, according to the model of Cox and Munk. The shape of the Gram-Charlier distribution is shown in Figure 3. This distribution is a slightly modified Gaussian, with width expressed by a sigma value similar to a Gaussian profile. In two dimensions the patterns are elliptical, with the long axis in the upwind-downwind direction. Designating the upwind-downwind sigma by σ_u, and the crosswind sigma by σ_c, the model developed here suggested that the ratio of laser return to that from a Lambertian water surface should be proportional to $1/\sigma_u\sigma_c$. More detail and the derivation of this relationship appear in Appendix A.

Glitter patterns were recorded by means of a video camera and a bright point light source at night, at the same time that radar altimeter signal measurements were recorded. The video recorded glitter patterns were later digitized along the major and minor axes of the ellipses and time-averaged intensity distributions obtained for the same periods over which the laser returns were recorded. The values of σ_u and σ_c were measured graphically from the plots of intensity. A pair of such plots is shown in Figures 4a and 4b.

2. Laser Return Signal Fluctuation

The laser radar altimeter at that time used a broader beam than the final model. it had a divergence of 1.2 by 2.4 degrees. This beam was incident on the center of the "glitter" pattern. The beam was treated as a pencil beam, essentially evaluating the peak value of laser return at the center of the glitter pattern. A consequence of the fairly narrow beam geometry was that reflection of the laser beam from the water surface occurred at a relatively small and finite number of glint facets. As a result, the laser return signal fluctuated rapidly with time over a wide range of magnitude. This required recording the signal for later data processing to obtain the mean and standard deviation of the variation. In order to accomplish the recording, it was also necessary to provide a pulse stretcher because the laser return pulses were otherwise too short to handle with most analog FM data recorders. A Hewlett-Packard model 3960A FM tape recorder was used to record the signals. The mean laser return signals and the standard deviation for each mean value were later determined from the FM tape recordings by processing in a DATA 6000 Data Processor.

At the time of the field measurements of the laser return from the water surface, measurements were also made of the return signal from a large white Lambertian surface, with a reflectance of 0.73 . This measurement was made with the transmitted beam horizontal, and with the Lambertian surface at a distance of 39 ft. This provided a reference signal for the system in the same configuration as used for water return.

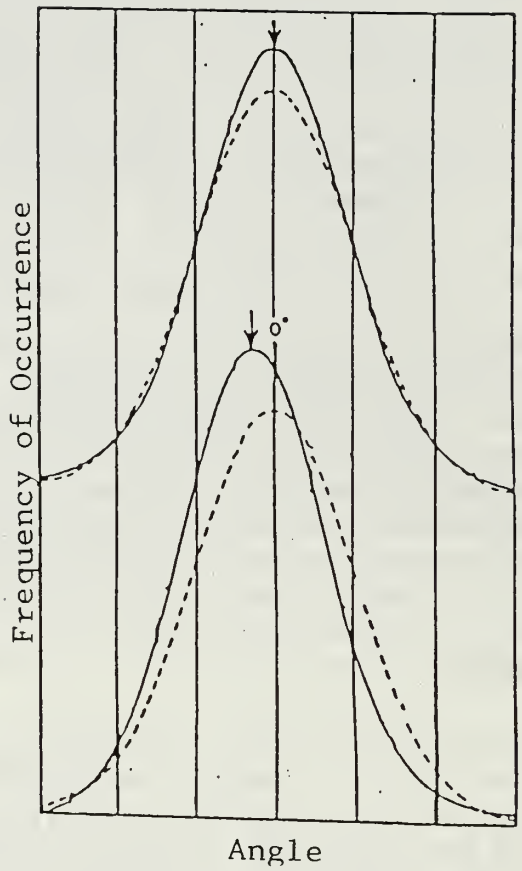

Figure 3. Wave slope distribution profiles deduced by Cox and Munk [Ref. 3]. Upper curves are taken along the Minor (Crosswind) axis of the elliptical pattern. Lower curves are taken along the major (up/downwind) axis. Solid curves are distributions deduced for a wind speed of 10 meters per second. Dashed curves refer to Gaussian distributions of the same standard deviation.

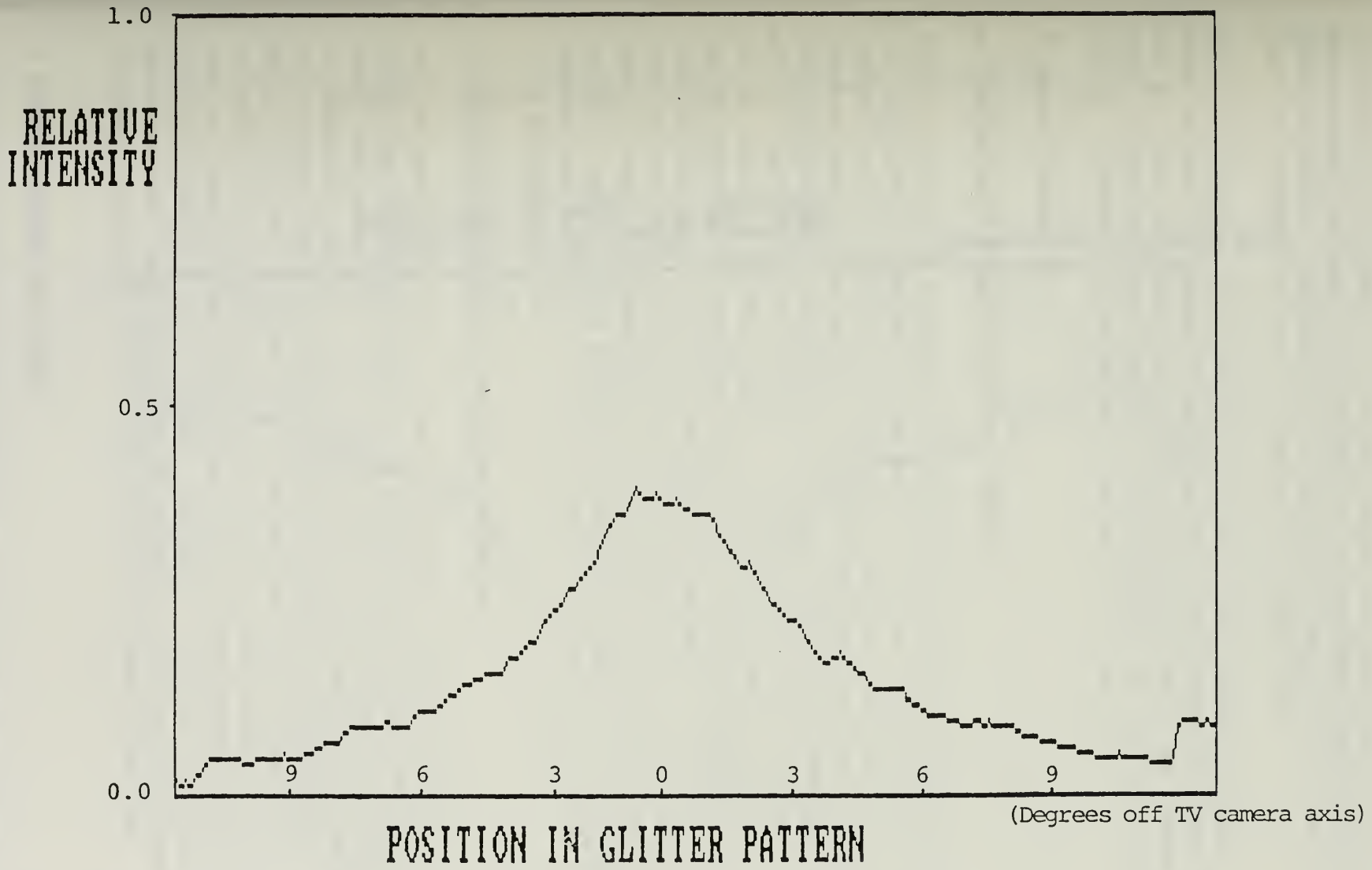

Figure 4a Upwind Glitter Pattern Intensity Profile

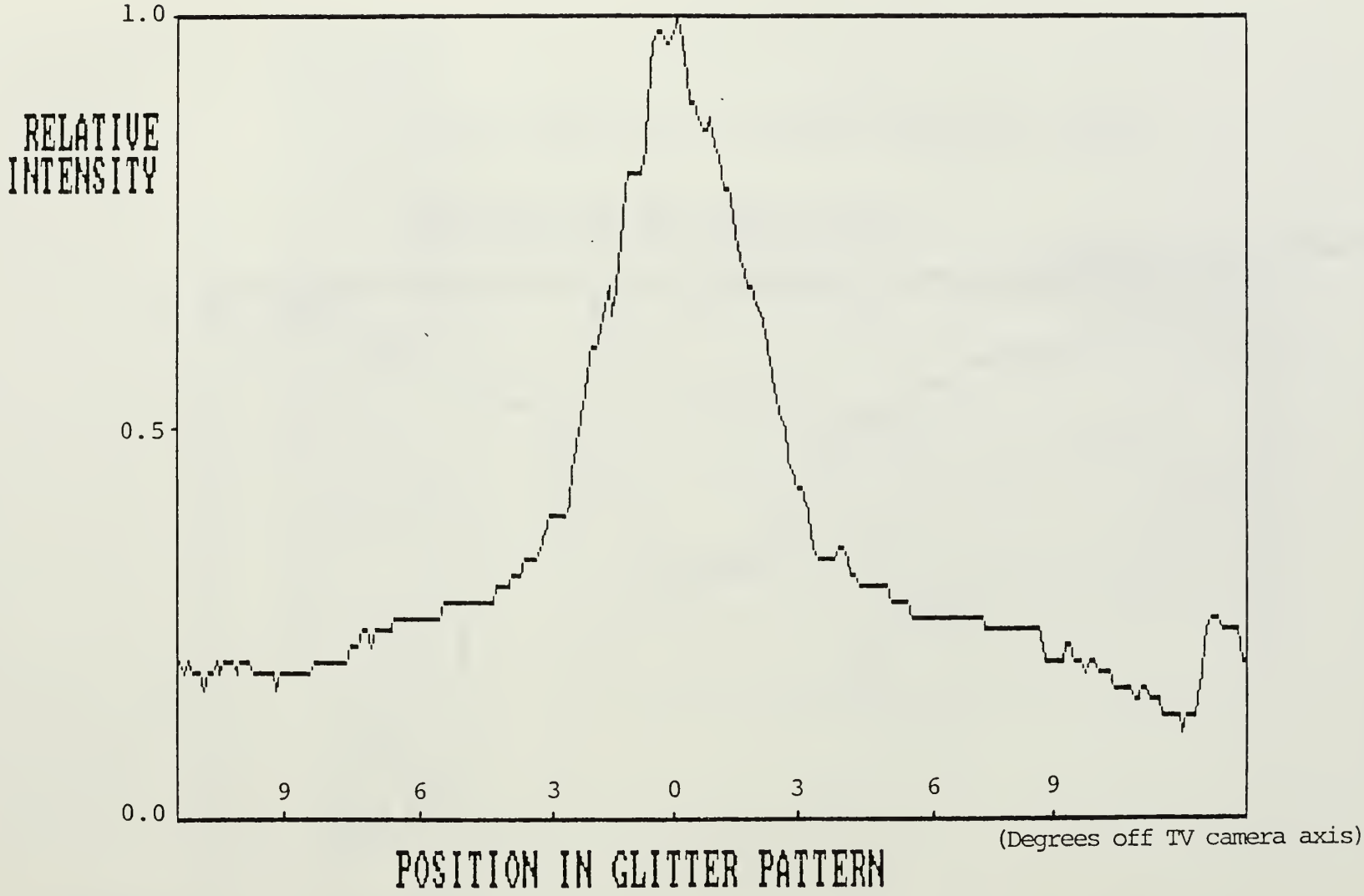

Figure 4b. Crosswind Glitter Pattern Intensity Profile

Although the rapidly fluctuating magnitude of the laser return posed a measurement problem, it is helpful in the practical application of a laser radar altimeter. Measurement of range is accomplished by determining the time delay between the primary pulse and the return pulse.

With fairly rapid pulse repetition rate, an occasional high pulse will serve to make the range determination practical, where the mean signal may not be above threshold for satisfactory operation. This feature tends to favor a small divergence beam. The statistics of this were not analyzed but are of interest and the tapes are available for future work.

3. System Calibration

a. Calibration by Means of Specular Reflection

Prior to the field experiments utilizing the glitter patterns, optimization of design and laboratory evaluation of the laser radar altimeter was often carried out using specular reflection from the surfaces of a plate glass window, after correction for the inevitable slight curvature of the window. This permitted some evaluation of the performance and permitted development of the time-difference circuitry. A rough evaluation of system performance can be obtained in this manner. However, the return signal is meaningful only if maximized by angular adjustment, and this evaluates only the peak value in the beam. A two-dimensional integration over the beam is necessary to make this technique quantitatively useful. Although rather unrelated to real field performance, it avoided the difficult problem of obtaining a rough water surface at sufficient range to be meaningful. The constant magnitude of the return signals in this situation was also helpful in the development work.

b. Calibration by Means of Lambertian Reflection

The problems attendant on use of specular reflection from a plate glass window are alleviated by use of a diffuse, "Lambertian" reflector such as a white sheet of paper. The signals with such a target are nearly constant in magnitude, except for a small amount of atmospheric scintillation. At close range, where the target is small enough to be manageable, the signals are so large as to make circuit development for small signal conditions difficult. Such calibration can be done at close range, by careful attention to quantitative attenuation of the large return signal that would otherwise saturate the receiver circuits. Prior to the glitter measurements reported here there was no definitive relationship between Lambertian laboratory measurements and the signals to be expected in field use.

4. Remote Sensing Test Results

A field test experiment was carried out from the Parrotts Ferry Bridge near Columbia, California, using the laser radar altimeter with parameters

listed earlier in this report. The distance to the water was 109 ft. The water was roughened by ripples with the laser return and the associated glitter pattern varying through a large range.

The measured values of σ_{eff}, the ratio of observed laser radar return to that expected for Lambertian reflection, are plotted as a function of the corresponding values of $1/(2\sigma_u\sigma_c)$, in Figure 5, where σ_u and σ_c are the measured upwind and crosswind Gram-Charlier standard deviation values for the glitter patterns. Use of the function $1/(2\sigma_u\sigma_c)$ for the abscissa was suggested by the model derived in this work. This functional form organizes the experimental points so as to fall fairly well along a straight line. The solid straight line is a least-squares solution for the data points, shown as the circles in that figure. The correlation coefficient is r = 0.96 for the points relative to this line. This line has a slope of 0.92 and an intercept of 44 on the ordinate axis.

The proposed model predicts a straight line through the origin with slope = 1.11 in Figure 5. This is represented by the dashed line in that figure. The existence of a theoretical model that would agree with the observed behavior in more detail would have been desirable, but the general trend indicated by plotting in this form is helpful.

The numerical values of σ_{eff} are of immediate utility. The lowest value, represented by the intercept on the y axis, is 44. Although extrapolation to the y axis has considerable uncertainty, it does imply that for the worst case the ratio of reflectance to that for Lambertian is considerably above unity, at least by somewhat over one order of magnitude. Without evidence such as this, a working altimeter would presumably have to be designed to cope with a worst case where a unity ratio to Lambertian might have occurred. This factor of 44, or somewhat over one order of magnitude increase in signal, represents a large reduction in the design requirement to be sure of a return signal.

The limiting value of σ_{eff} of 44 for extremely rough water is consistent with results summarized by Cox and Munk, including much earlier work, that quoted the maximum wave slope ever encountered as about 30 degrees. Since the shape of glitter patterns is Gram-Charlier, or nearly Gaussian, it takes an educated guess to interpret the meaning of cutting off at 30 degrees. However, if the cutoff is taken to be the 2 sigma point, and the pattern has a minor axis half the major axis, then with the sigmas in radians, $1/2\sigma_u\sigma_c = 29$. Using the solid line of Figure 5, the best-fit line for the data points on that curve, this abscissa value would give a value of σ_{eff} of 68. This is in general agreement with the value 44 for the intercept. At any rate this indicates that there is a cutoff for extremely rough water.

That the observed signals are directly relatable to reflection from a Lambertian surface, makes it possible to do most of the testing work in the laboratory. Various evolutions of laser radars can then be tested with a

Lambertian surface, such as a white sheet of paper. The signals can be scaled to those for a water surface at any required distance, and the "worst case" evaluated. The present experiment has achieved the objective of providing a means of determining the optical state of the rough water by a remote sensing technique. The result is semiempirical, but is useful.

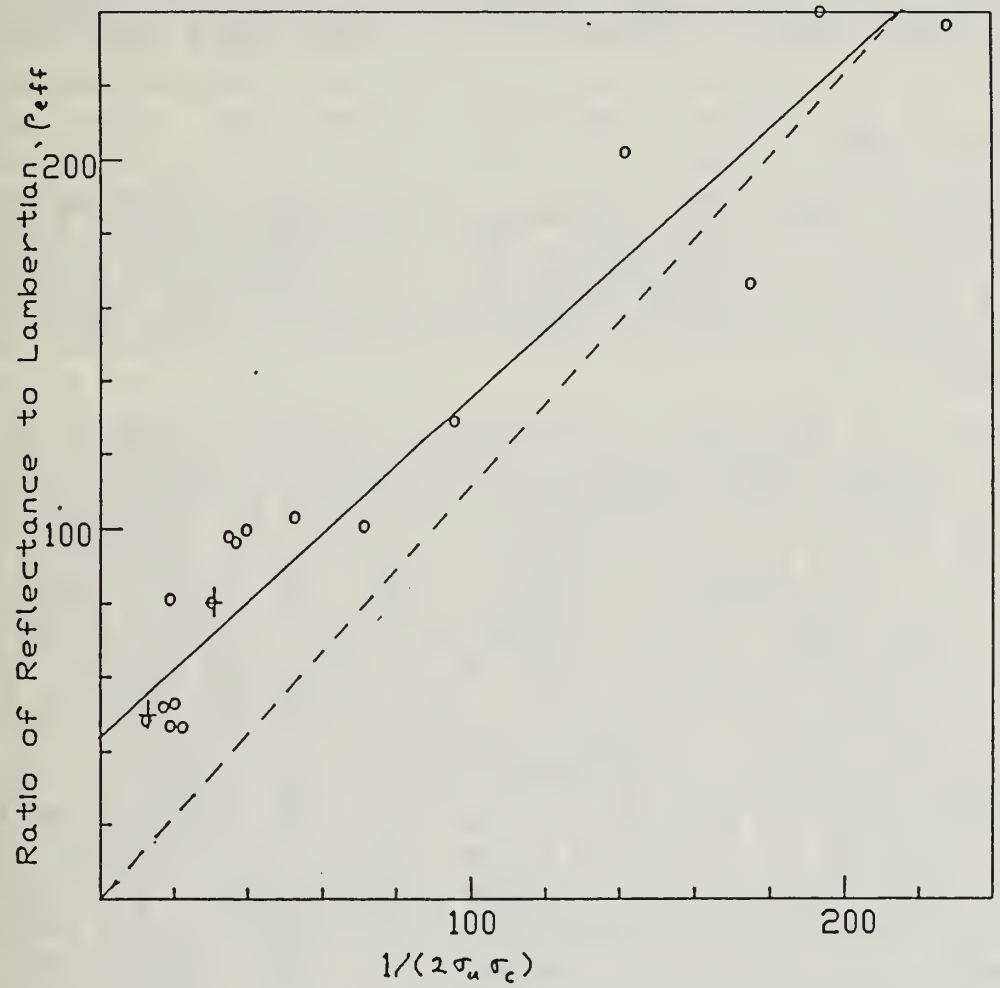

Figure 5. Observed effective reflectance relative to Lambertian, ρ_{eff}, as a function of $1/(2\sigma_u\sigma_c)$, plotted as circles. The solid line is a least squares fit of a straight line to these points. Two data points plotted as crosses are based on Petri's data [Ref. 2]. The dashed line represents an ideal model proposed in this thesis.

V. REFLECTED SUNLIGHT NOISE TESTS

1. Field noise tests

As discussed in section lV of this report, the amplitude of the returned laser signal from the "worst-case" rough sea state is the equivalent of reflection from a Lambertian surface, but with a reflection coefficient of 44 times the reflectance of a water surface. This gives a Lambertian reflectance of

$$44 \times .0204 = 0.89 \quad .$$

A white sheet of paper has a Lambertian reflectance of about 0.75 at a wavelength of 904 nm. Consequently most of the calibration values were obtained with such targets, or equivalent paper, and the return signal, corrected by the ratio 0.89/0.75, taken to be that from the "worst case" rough sea state.

Measurement of the shot noise produced by the current flowing in the avalanche photodetector under "worst-case" sea state conditions and with the sun directly overhead, was simulated by arranging the detector optical system so as to view, at normal incidence, a white piece of paper in direct sunlight. The measurements were made at solar noon at 36 degrees north latitude at dates near the summer solstice when the sun is at about 22 degrees north latitude. The sun is thus at an angle of 14 degrees from the vertical. Vertical sunlight intensity at 904 nm. exceeds that for a path 14 degrees from vertical by only 0.3%, using data from the 1974 RCA Electro-Optics Handbook, so that correction has been neglected. The white paper was inclined at 14 degrees from the horizontal, perpendicular to the sunlight. The noise was measured at the output of the amplifier at the point where the signal is applied to the trigger system. The noise was measured on a Hewlett-Packard Model 4300A true RMS meter with a bandpass of 10 Megahertz. The noise includes components to about 1 Megahertz. The noise measured 0.325 volts RMS. Corrected for the relative reflectance, 0.75, for the paper, to that for the "worst-case" rough water reflectance, 0.89, gives a solar noise of 0.386 volts RMS. This noise value is slightly below the maximum noise, 0.410 volts RMS, as limited by the feedback regulation on the avalanche photodiode.

2. Signal Plus Noise Tests

ln order to fully simulate the performance of the system under maximum solar reflection conditions, the system was set up so that the receiver was illuminated with light to bring the noise to a value of 0.386 volts RMS, simulating worst-case sunlight, at the same time that laser return pulses were received. The gain limiting circuit was set to limit at 0.421 volts RMS noise. As this limit is rather close to the noise, a reduction in gain by a factor 0.8 was expected on the basis of a measured voltage drop of 1.2

volts at point A relative to Point B in Figure 2. This translates to a 3.2 volt drop at the avalanche photodiode because of the resistor R_1

VI. FALSE ALARM RATE TESTS

The false alarm rate tests were made with a noise signal set at 0.410 volts RMS. This noise signal was produced by illuminating the receiver with a quartz halogen lamp and focusing lens. The lamp was operated on a regulated dc power supply. The maximum noise signal permitted by the regulating system in the receiver was .415 to about .430 volts depending on the length of preceding warmup of the system. The noise started at the higher value and settled slowly to the lower value. The noise of 0.410 volts RMS was maintained on the low light side of the maximum noise peak. With the noise fixed at 0.410 volts, the trigger threshold was set at a series of values and the number of triggering events counted on a nuclear pulse counter. The results are shown in Figure 6, with count rate as the ordinate and height of the input pulse for triggering as the abscissa. The upper curve is for triggering with a single pulse. The lower curve is for triggering with the requirement of a pulse in two consecutive time windows. The data for the upper parts of the two curves were taken with a window time length of 2.25 microseconds. The count rate for this window time length became prohibitively long as the trigger threshold was increased, so the time window was increased to 490 microseconds. For the single pulse count rate the rate increase was proportional to the fractional increase in time window length. For the double pulse counts, the rate increase was proportional to the square of the fractional increase in time window length, as expected. The count rates plotted in Figure 6 have been divided by the time window ratio for the single pulse curve and by the square of that ratio for the double pulse curve. The entire curve is thus the equivalent of a curve for a 2.25 microsecond window. The large increase in the count rate with the longer time window permitted measurements at higher trigger levels where the count rate with a small time window would be immeasurably small. The vertical error bars represent the $\pm$ sigma uncertainty in the statistics of counting. For the points taken with the 490 microsecond window the vertical uncertainty due to counting is negligible. For all the points, the uncertainty in trigger threshold setting is about the same, as indicated by the horizontal error bars.

It can be seen from Figure 6 that use of the double pulse requirement decreases the false alarm rate by a large factor, relative to single pulse triggering, approaching 10^{-5} near the operating threshold of 3.2 volts at the lower end of the double pulse curve. The operating time window for much of the test data was taken with a 2.25 microsecond window. In the final model, the time window will be reduced to about 100 nanoseconds, and will be movable to center at whatever triggering time is selected. This factor of 22.5 reduction in time window will lower the false alarm rate by a factor of $(22.5)^2$, or about 500. The false alarm rate for the 2.25 microsecond window is about 10^{-4} at an operating trigger threshold of 3.0 volts.

Use of a 100 nanosecond window will produce a false alarm rate of 2×10^{-7}. This translates to one false alarm in about 5×10^{6} seconds or one false alarm in 80,000 parachute descents of 60 seconds duration.

The choice of trigger threshold setting is quite arbitrary. A slight increase in that setting will decrease the false alarm rate sharply, but will decrease the maximum usable altitude only slightly. For example a change of trigger threshold setting from 3.0 to 3.2 volts will decrease the false alarm rate by about a factor of 10 while reducing the range by $(3.0/3.2)^{1/2}$, or 3%.

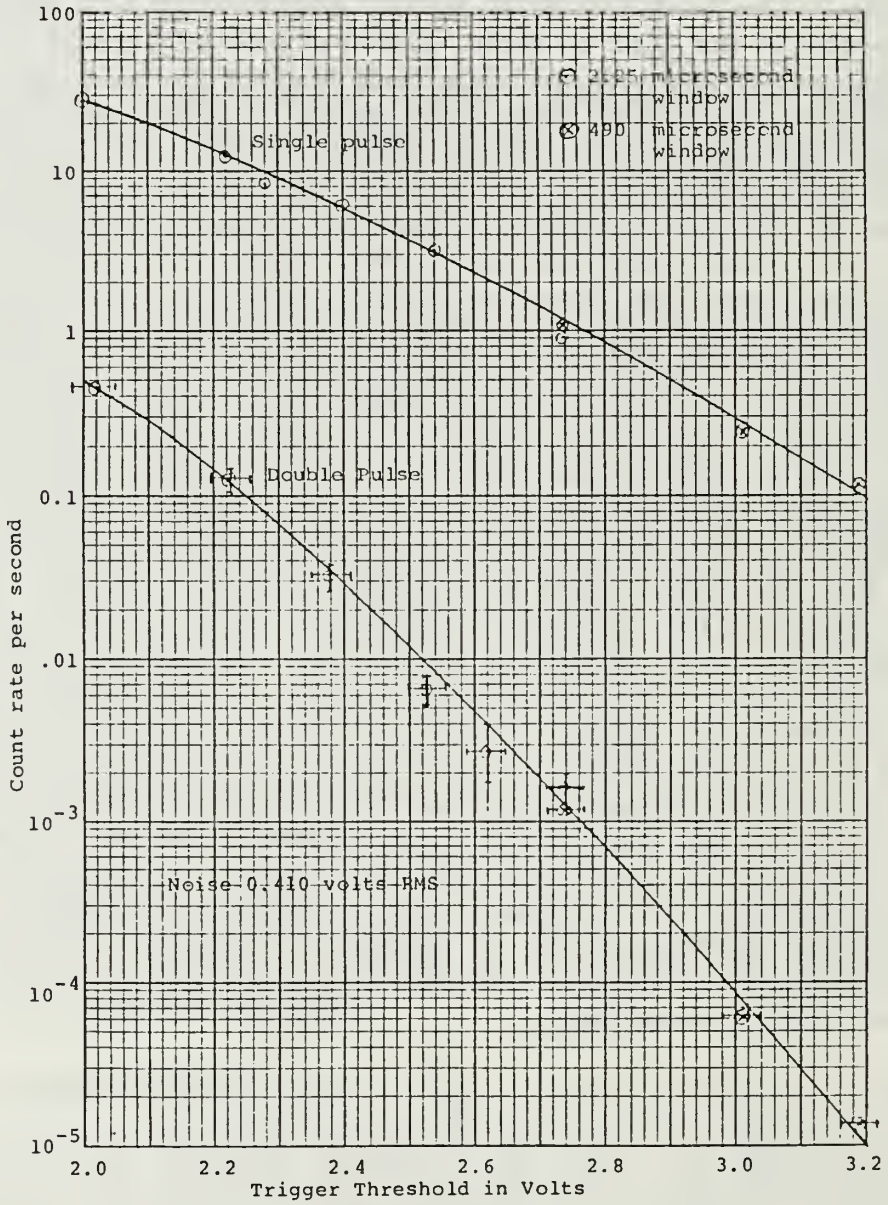

Figure 6. Noise triggerings as a function of threshold

VII. "TRIGGERING" ALTIMETER SYSTEM TESTS

The "triggering" altimeter system was set up on a test range on the eighth floor roof of Spanagel Hall at the Naval Postgraduate School. The eighth floor exists only on the two ends of the building, with an unobstructed region at seventh floor level between. Use of this range was approved in advance by the NPS Laser Safety Review Board as meeting ANSI laser safety requirements. The range was 69 meters in length. Performance of the laser altimeter system at longer ranges was inferred from the return signals measured on that range. A few verification measurements were also made at longer range on a previously approved path from the transmitter site on Spanagel Hall to a Satellite dish of unknown reflectivity on Root Hall, at a range of about 180 meters.

For use in the field, it is more convenient to use a large sheet of reinforced "boxboard" than a white sheet of paper because the boxboard will stand up in a light wind with minimal support. The reflected amplitude at 904 nm. from such a sheet of brown boxboard was compared with the reflected amplitude from a white sheet of paper and found to have identical reflected amplitude. Consequently most of the laser return signal measurements were obtained with such targets and the return signal taken to be that from the "worst case" rough sea state.

Table II presents the results of measurements made with the final model. The signals at full laser voltage and full avalanche voltage were so high as to be clipped at the limiting 6 volt level, although the leading edge is perfectly satisfactory for triggering. In order to evaluate the equivalent unclipped signal voltage that would correspond to full gain and full laser voltage, the laser voltage and the avalanche voltage were adjusted to keep the return signal at 4.0 volts. Previous calibration of the laser power at lower voltages and the avalanche gain at lower voltage allowed calculation of the equivalent return signal. The last column in the table presents the calculated range at which the return signal would be equal to the trigger threshold level of 3.0 volts. The value quoted at the foot of this column is the range value for the automatic gain control in operation with simulated worst-case sunlight.

Table II. Calculated ranges for which the return signal would be equal to the 3.0 volt trigger setting, based on measurements made on a 69 meter range, in the absence of solar noise. The final value is corrected for gain regulation due to noise, for overhead sun and the worst-case sea state.

Return Signal (Volts)	Avalanche Voltage	Avalanche Relative Responsivity	Laser Voltage	Laser Relative Power	Equiv. Signal, Volts	Calculated Range for 3.0 V Sig. (Meters)
---	226 (Max. Avalanche)	1.00	101 (Max. Laser)	1.00	---	---
4.0	209 (High Avalanche)	.400	60 (Low Laser)	.105	95	389 m
4.0	178 (Middle Avalanche)	.140	70 (Middle Laser)	.254	112	422 m
4.0	148 (Low Avalanche)	.070	80 (High Laser)	.481	119	434 m
				(Low Noise) Mean Range -->		415 m
				Worst-case sea-state solar noise limited mean range -->		371 m

For operation with the worst-case sea state and the sun directly overhead, the noise voltage is expected to be .386 volts. This is near enough to the limiting noise signal set by the present circuit (0.410 volts) that the limiting circuit has begun to reduce the gain. The measured gain is reduced to .80 of the full gain. This reduces the maximum usable altitude, by a factor square root of 0.8, from 415 meters to 371 meters.

For the alternative optical system, with more nearly optimized optics, the solar noise would be reduced by about a factor of two and the signals increased by a factor somewhat in excess of 4, yielding a range of approximately 800 meters. That system would have an acceptance cone angle of about 1/2 degree. That alternative optical system has not yet been tested.

The "worst-case" sea state utilized above represents use of the reflectance value of 44 predicted by the work carried out on the Parrot's Ferry Bridge over the New Melones reservoir. Since these results were extrapolated from data on small waves, the behavior for actual open ocean waves may be different. Work is progressing for waves under the Golden Gate Bridge and later measurements are planned for use of a helicopter over the ocean. Until these results are available the present results must be considered tentative.

VIII. "READOUT" LASER ALTIMETER

1. Basic Concept

The "readout" laser altimeter differs from the "triggering" laser altimeter in that the time of arrival of a return pulse for the "readout" altimeter is converted into a dc voltage that is proportional to the altitude. The altitude "readout" circuit triggers for every laser pulse that returns from the water surface. In contrast to this, the "triggering" laser altimeter triggers, so as to initiate deployment of some package, only if the elapsed time is equal to the preset round-trip time for the altitude desired.

The "readout" circuit employs a linear ramp voltage which is fed into a sample-and-hold circuit. The sampling takes place at the time of arrival of the return pulse. The output of the sample and hold circuit is a voltage, v, and the altitude is given by

$$h = (50.00 \text{ meter per volt}).v$$

The laser fires at a 1 kilohertz rate. The voltage v holds until a few usec before the next laser firing. Thus, if there is a return signal from every laser firing, the time delay for each will be constant and the readout output will be a series of level voltages and a digital voltmeter can be used as an output meter. If return signals are missed, the readout is designed to give a zero output. For the case of appreciable missed return signals, an oscilloscope can be employed to monitor the output.

2. Laboratory test results

The readout circuit was calibrated with test pulses of constant amplitude. The solid line of Fig. 7 is the measured output (converted to meters using 50.0 meters/volt) plotted as a function of the accurately known input in terms of meters. The deviation from direct linearity below 20 meters input is due to the non-linearity of the ramp waveform generator. This curve was obtained by using the readout test pulser, a digital voltmeter at the altimeter readout output, and an oscilloscope accurately calibrated in time. For a test pulse of constant amplitude, the curve of Fig. 7 is accurate to within 1 meter.

3. Field test results

The principle test of the readout package with the laser altimeter was made on the test range on the roof of Spanagel Hall. The results of this test also appear on Fig. 7. In this case, the abscissa of Fig. 7 represents the horizontal distance from the laser altimeter and receiver to the reflector, a sheet of cardboard. Points 1,2,3,4 correspond to readout output distances for the corresponding directly measured distances to the movable target.

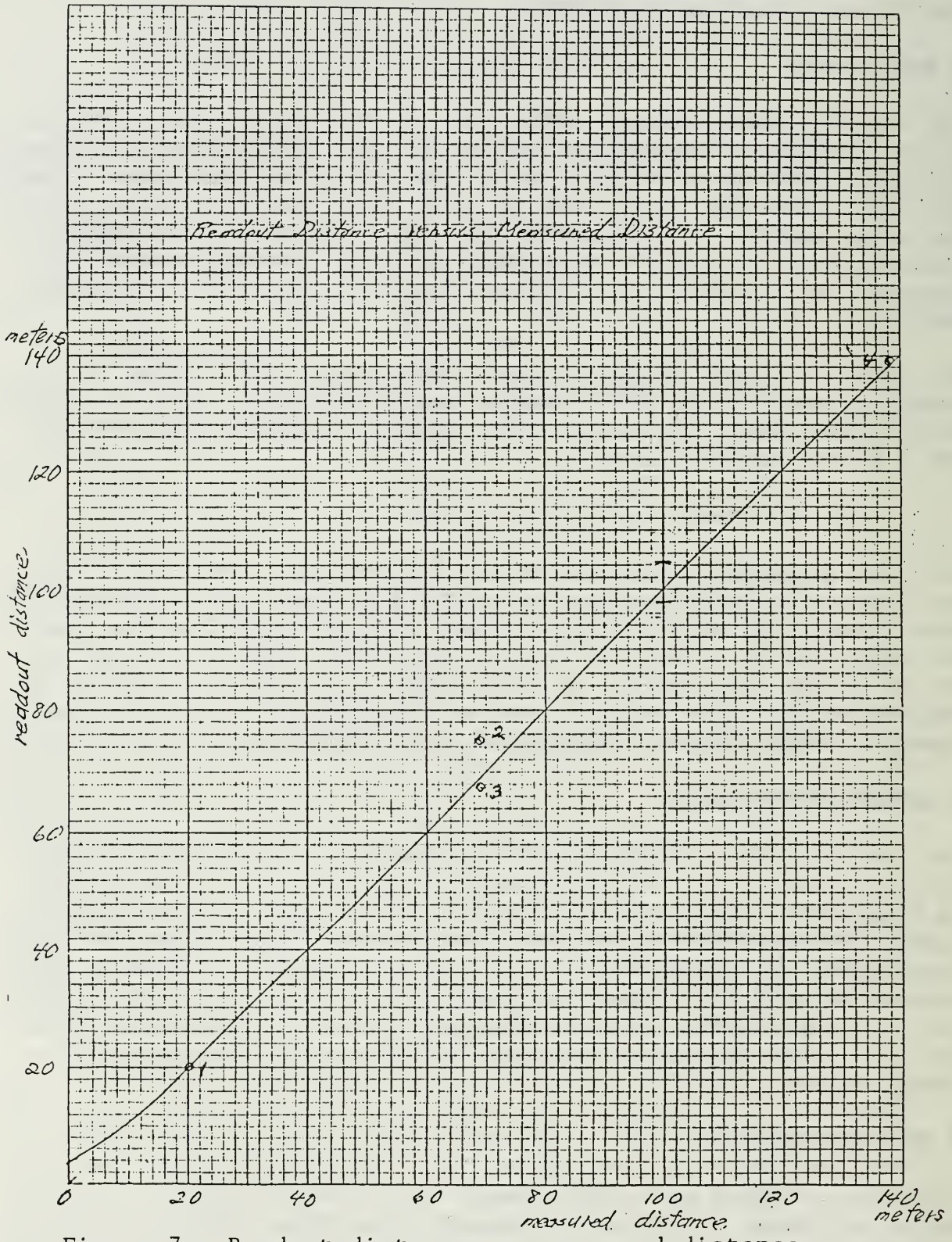

Figure 7. Readout distance vs. measured distance

The error bar shown at 100 meters input distance illustrates the uncertainty in readout due to the variation in amplitude of the return signal using the original "leading edge detector". The upper portion corresponds to input pulses between 3 and 4 volts amplitude; the lower portion corresponds to input pulses between 4 volts and saturation (6.75V). These measurements were made using the readout test pulser.

Point 1 was a calibration point formed by adjusting the readout circuit to give a 20 meter output at a known distance of 20 meters.

Point 2 was obtained for a target distance of 69 meters by using a corner cube to reflect the beam back to the detector. Because of the high intensity of the reflected light, a very low detector sensitivity was used. In normal use, the laser altimeter would not operate with such a low sensitivity.

Point 3 was obtained by reflecting from a cement wall (at the same distance as point 2). Here the highest detector sensitivity was used. Subsequent lab measurements have shown that low sensitivity detector pulses are delayed relative to high or moderate sensitivity detector pulses. This accounts for the relatively large positive deviation of point 2 from the solid line of Fig. 7.

Point 4 was obtained at a distance effectively twice that for points 2 and 3. This was done by placing a plane mirror at 69 meters and reflecting the laser beam back to a corner reflector near to but offset from the laser. A second round-trip reflection then takes place resulting in a doubling of the original distance to 138 meters. A medium detector sensitivity was used for this measurement.

The results of this test and measurements using the readout test pulser indicate that the readout performs according to its design predictions.

Details of the readout circuitry and its calibration and adjustment appear in Appendix B.

APPENDIX A, MEASUREMENT OF OPTICAL SEA-STATE

1. INTRODUCTION

Evaluating the performance of the existing working model of a laser radar altimeter system over the water had the problem that the reflectance of a water surface is dependent on the roughness state of the water. The only data in the literature known to this author, which would permit an estimate of the laser reflectance of rough water, are those of Petri [Ref.2]. These data are rather meager, consisting of 16 separate measurements, and requiring a knowledge of the wind speed. The latter had been measured at a height of 60 feet above the water. The wind speed at the water surface was thus quite uncertain. Other data by Cox and Munk [Ref.3] related the glitter pattern profile, for reflection of the sun, to wind speed over the ocean. Their optical data were taken from an aircraft at 2000 feet altitude, with windspeed measured on a ship at two heights, 9 feet and 41 feet above the water. It was not clear which of these two heights was used for quoting the wind speed. Their data also were not directed at evaluating the magnitude of the reflectance.

2. GENERAL OBJECTIVE

Preliminary field experiments, carried out as part of the work reported here, indicated that the reflectance of rough water could vary rapidly under changing wind conditions, and that knowledge of the wind speed at a given instant did not serve as a good indicator of the optical properties of the water surface at that instant. Additionally, if wind speed were to be measured, it probably should be measured very close to the water surface. This would be difficult, expensive, and in many cases impractical. The field work reported here for this project was carried out from high bridges, but it was intended that the work would be extended later to aircraft. In that case the necessity for associated ship measurements of wind speed would be difficult logistically. Consequently, the objective of this work became to develop and demonstrate the feasibility of a remote sensing technique for evaluating the reflectance of a rough water surface at the instant of a laser radar altimeter test.

The papers of Cox and Munk, and Petri, taken together, led to a conclusion that it might be possible to predict an expected laser radar return on the basis of a measurement of the width of glitter patterns. It also seemed likely that glitter patterns measured with a nearly point source of light at night would be simpler to obtain and would yield more directly the desired result than would glitter patterns obtained with the necessarily oblique illumination from the sun. Consequently, the primary objective became to test the feasibility of prediction of laser return from the profile widths of glitter patterns obtained with a point light source. The early tests indicated that laser return was in fact a function of glitter pattern width. A tentative theoretical model was developed, which, although it has not as yet succeeded in predicting the observed absolute magnitude of laser return, does lead to a functional relationship which is useful. With the present semiempirical relationship, laser return can be related quantitatively to Lambertian return. Although more experimental data is needed to refine the results, and further theoretical work is needed to clear up the discrepancy in the absolute values predicted by the

model, laser return signals measured in the laboratory with Lambertian targets can now be directly related to field-expected values.

3. ASSOCIATED PROBLEMS

a. Laser Return Signal Fluctuation

There were several additional problems in carrying out the field experiments at the outset of this project. The laser radar altimeter model to be tested used a fairly narrow laser beam of 1.2 by 2.4 degrees divergence, with a 3 degree circular cone of acceptance of the receiver optics. This divergence had been chosen in the design process of the companion project as an optimization of the transmitter-receiver optics under the confines of required return signal magnitude and availability of inexpensive commercial components. This narrow beam was incident on the center of the "glitter" pattern, about which much more will be said later. The beam will be treated here as a pencil beam, essentially evaluating the peak value of laser return at the center of the glitter pattern. A consequence of the narrow beam geometry was that reflection of the laser beam from the water surface occurred at a relatively small and finite number of glint facets. As a result, the laser return signal fluctuated rapidly with time over a wide range of magnitude. This required recording the signal for later data processing to obtain the mean and standard deviation of the variation. In order to accomplish the recording it was also necessary to provide a pulse stretcher because the laser return pulses were otherwise too short to handle with most analog FM data recorders.

Although the rapidly fluctuating magnitude of the laser return posed a measurement problem, it is helpful in the practical application of a laser radar altimeter. Measurement of range is accomplished by determining the time delay between the primary pulse and the return pulse. With fairly rapid pulse repetition rate, an occasional high pulse will serve to make the range determination practical, where the mean signal may not be above threshold for satisfactory operation. This feature tends to favor a small divergence beam. The statistics of this were not analyzed here but are left for later work. The data tape recordings from the field experiments are now available for such analysis.

b. Calibration by Means of Specular Reflection

Prior to the work reported here, optimization of design and laboratory evaluation of the laser radar altimeter had been carried out primarily using specular reflection from the outside of a plate glass window to obtain a return signal, after careful measurement of the inevitable slight surface curvature of the window. This permitted development of the time-difference circuitry and avoided the difficult problem of obtaining a water surface at sufficient range to be meaningful. The constant magnitude of the return signals in this situation was also helpful in the development work. In evaluating the magnitude of the signal, the difference of reflectance of the two glass-air interfaces from that of a single water surface was easily accounted for. A rough evaluation of system performance was obtained in this manner, but the return signal, if maximized by angular adjustment to obtain the maximum signal, evaluated only the peak value of

the central maximum of the laser beam. To obtain a measure of the expected return signal from a rough water surface or a diffuse reflecting surface from the specular reflection data required carrying out a two-dimensional integration of the laser beam flux over the laser beam cross-section profile. The beam tended to have considerable detailed "banding" structure in its profile, making such evaluation rather doubtful.

c. Calibration by Means of Lambertian Reflection

The problems attendant on use of specular reflection from a plate glass window to obtain a return signal are alleviated by use of a diffuse, "Lambertian" reflector such as a white sheet of paper. For a finite area, such a surface reflects a power proportional to the cosine of the angle of incidence. Such surfaces were used in the laboratory. However, the Lambertian surface must be large enough to include the entire transmitted laser spot. Hence at ranges sufficient to simulate real field conditions, the area required was large enough to make obtaining a good uniform reflectance white surface difficult. The signals with such a target would be constant in magnitude, except for a small amount of atmospheric scintillation. At close range, the signals were so large as to make circuit development for small signal conditions difficult. Calibration of the return signal magnitude can be done with a Lambertian surface at close range, by careful attention to quantitative attenuation of the large return signal that would otherwise saturate the receiver circuits. This sort of calibration was done in the field tests to be reported here. Finally there seemed to be no fully satisfactory way to simulate all the circumstances to be encountered by a real life laser radar altimeter, other than by field tests over wind-roughened water. These were then initiated and the accompanying remote sensing techniques reported here carried out.

4. GENERAL METHOD

This work reports a new remote sensing system for estimating the expected laser radar return signal through analysis of glitter patterns. This is a remote sensing method permitting determination of the expected reflectance of a rough water surface using equipment colocated with the laser radar altimeter. The equipment for this technique also offers the advantage of being inexpensive and physically small for field use.

The time-averaged statistical distribution of light intensity was measured for images of glitter patterns produced by reflection of light projected onto the water from a small area incandescent source located near the laser altimeter. The images of the glitter patterns were recorded with a video camera, which avoided the nonlinearities of photographic recording and permitted digitization without intermediate steps. The magnitude of the returned laser signal was recorded at the same time that the video images were obtained. Because this signal was rapidly varying, it was recorded for statistical processing later. The resulting data related the mean laser return to the glitter pattern profile parameters. The results are most succintly expressed as a ratio of reflectance of the rough water to the reflectance of a (virtual) Lambertian reflector which reflects the same fraction of the total light as a water surface (0.0204) at normal incidence. Through use of data in other references, the return was also

related to an inferred wind velocity for comparison. An analytical model was developed which seems to predict the correct functional behavior, although the predicted absolute magnitude of reflectance is at present out of line. Although these experiments should be repeated for refinement and completion, these results allow evaluation of a practical laser radar system by reflection from a Lambertian reflector within the laboratory, providing a more immediate and readily controlled environment for equipment development.

5. THEORETICAL CONSIDERATIONS

a. General

When light from a small diverging source is incident on a water surface roughened by wind driven waves, it is reflected from the water surface in a glitter pattern, as seen by an imager located near the source. The glitter pattern is approximately elliptical in shape, with the major axis of the ellipse in the upwind direction, and the minor axis in the crosswind direction [Ref. 4]. The pattern is produced by specular reflection at a large number of rapidly changing facets located at the points where the surface is perpendicular to the incident light. A representative glitter pattern is shown in Figure 8.

Laser reflectance from calm waters can be readily calculated analytically [Ref. 5]. This is the case of specular reflection whereby a mirror image of the source is created equidistant below the water surface. Reflected energy appears to originate from this source.

At the other extreme from specular reflection is diffuse reflection. In this case a surface scatters incident energy over all angles in a hemisphere, resulting in a distribution called Lambertian, in which the reflected energy varies as the cosine of the angle from the perpendicular.

Between these two extremes, an optically rough water surface exhibits properties of both types of reflection. The reflected intensity distribution varies according to the distribution of wave slopes scattering the incident beam. [Ref. 6].

b. Glitter Patterns

The technique developed in this work was a method of evaluating the expected laser radar return from a water surface when it is roughened by wind. The technique is a remote sensing technique in that all measurements are made from the general location of the laser radar altimeter. Thus it does not involve knowing the windspeed at the water surface, nor any other meteorologic or oceanographic parameters. The measurements involve only the optical properties of the water surface. This is done by determining the size of the glitter pattern from a video camera recording of the reflection of an approximately point source of light near the laser radar. The laser radar used a pencil beam, so that it responded to the central maximum reflection point of the glitter pattern profile. The reflection from this fluctated through a large range, as a function of time, so that a time-average of a recorded signal was required.

Figure 8. Glitter pattern produced by wind speed of approximately 12 mph.

Cox and Munk have developed a method of measuring water surface roughness from photographs of sun glitter [Ref. 3]. The wave slope distribution was deduced from observations of sun glitter patterns, with the assumption that the wave slope distribution and the reflected light intensity distribution were the same. They found that a Gram-Charlier distribution was the best fit to the experimental data. This distribution function is

$$G = [1/(2\pi\sigma_u\sigma_c)] \times e^{-(X^2+Y^2)/2} \times$$

$$[1 - (1/2)\,C_{21}(X^2-1)Y - (1/6)C_{03}(Y^3-3Y) \quad \text{<-Skew}$$

$$+ (1/24)C_{40}(X^4-6X^2+3)$$

$$+ (1/24)C_{04}(Y^4-6Y^2+3) \quad \text{Peakedness}$$

$$+ (1/4)\,C_{22}(X^2-1)(Y^2-1) + \ldots]$$

$$\text{or,} \quad G = [1/(2\pi\sigma_u\sigma_c)] \times e^{-(X^2+Y^2)/2} \times [H] \qquad (1)$$

where $X = \Theta/\sigma_u$ with Θ the angle from vertical in the upwind/downwind direction, and

$Y = \Phi/\sigma_c$, with Φ the angle from the vertical in the crosswind direction.

The quantities σ_u and σ_c are the upwind and crosswind "standard deviations" for this distribution. For a Gaussian distribution the standard deviation is the root mean square deviation from the mean. The first two terms of the Gram-Charlier distribution are the same as for a Gaussian distribution. The Gram-Charlier sigma values are the values of sigma in the second term. As will be discussed later, the peakedness of the Gram-Charlier distribution causes these sigma values to be located lower on the curve than for a Gaussian distribution. The terms in the brackets in the Gram-Charlier distribution are a form of Hermite polynomial. These terms express the peakedness and skew of the function.

The Gram-Charlier distribution, above, is a two dimensional distribution. It is displayed as a function of Θ and Φ in Figure 8. (See section IV) The dotted curves are the shape of a Gaussian with the same standard deviation values. The crosswind distribution is symmetric about the vertical but is more peaked than Gaussian. The upwind distribution is also more peaked than Gaussian, and has a skew in the upwind direction.

The Gram-Charlier distribution is a normalized function, i.e., with the complete Hermite polynomial series included, the integral of the function from minus infinity to plus infinity in X, and from minus infinity to plus infinity in Y, gives unity. At first sight it would seem that integration from minus infinity to plus infinity, over the angular variables used, is not strictly correct, as the angles can only go to $\pi/2$. The function as written above is an approximation, as it has only the first few terms of the Hermite polynomial included. However, Cox and Munk stated that this approximation was valid for all their data out to X = Y = 2.5. Contributions to the integral for values of X and Y beyond 2.5 are negligible, so that writing the integral as if it extended to infinity should be of no concern. The largest sigma values encountered in the data reported

here were 7.5 degrees. For X = 2.5 this means the expression is taken to be valid to 19 degrees. The integrals written later in this report will express the limits as minus infinity to plus infinity, recognizing that the contributions of high X and Y are negligible.

The extent to which the Gram-Charlier distribution exceeds the Gaussian due to the peakedness at the center can be evaluated by inserting the values of the coefficients, as given by Cox and Munk, and letting X = 0 and Y = 0. For the crosswind direction, the curve has no skew and the peakedness is independent of wind velocity. The coefficients for crosswind peakedness are

$$c_{40} = 0.40 \pm 0.23 ,$$

$$c_{04} = 0.23 \pm 0.41 , \qquad (2)$$

and $$c_{22} = 0.12 \pm 0.06 .$$

This gives a term multiplying the value of the peak as given by the first two terms of equation (1), i.e. the height of the Gaussian central peak is multiplied by a factor of

$$f = 1.109 \pm 0.061 . \qquad (3)$$

This factor will be used as 1.11 later.

For the upwind direction the skewness constants are

$$c_{21} = 0.01 - 0.0086W \pm 0.03 ,$$

and $$c_{03} = 0.04 - 0.033W \pm 0.12 , \qquad (4)$$

where W is the wind speed in meters per second. Although these constants depend on wind speed, they do not affect the area under the curve, and hence the normalization, as X and Y appear only in odd powers in the Gram-Charlier Hermitian terms. Thus whatever area they add for positive values of X or Y, they subtract for negative X or Y.

Although the skewness terms do not affect the peakedness for the crosswind direction, they do make a small contribution to the peakedness in the up/downwind direction, but the contribution is small. For example, for a wind speed of 10 meters per second, as illustrated in the lower curve of Figure 2, the additional peakedness is approximately two percent. The position of the peak is also shifted slightly upwind. However, its position is still within the "pencil" beam of 1.4 x 2.8 degrees used in the laser radar altimeter here. The values for the predicted laser return signal presented later in this reporthave been adjusted for the skewness contribution to the peakedness, even though this adjustment is in most cases the order of one percent - really negligible in view of the 6 percent uncertainty quoted above from Cox and Munk on the value of the peakedness factor.

To return to the meaning of the "standard deviations" for the Gram-Charlier distribution, the standard deviation values, σ_c and σ_u, are the standard deviations of the Gaussian term of the Gram-Charlier form. In

measuring these quantities on an actual measured distribution, as will be described later in this work, it is necessary to measure the distribution curve width at a point lower by a fraction 1.11 (or 1.12, depending on the skew contribution to the peakedness for that particular curve) than the usual 0.659 times the peak value - the case for the usual Gaussian distribution. This has been done in evaluating the data later in this thesis.

A further fine tuning should also be noted. The peakedness terms in the Gram-Charlier distribution do produce upward, or downward, displacements of the curve throughout the curve. This can be seen in the curves presented in Figure 1. Because of this displacement, it might seem that determination of sigma values by measuring the width of the peak at a height equal to 0.659/1.11 times the peak value, would be in error. (The factor 1.11 comes from equation (3) above.) To evaluate this effect, the coefficients in equation (2) above produce vertical displacements of the crosswind curve, i.e. for $Y = 0$, at $X = \pm 1$ (at the σ_c point), given by

$$
\begin{aligned}
& 1 + (1/24)\, c_{40}\, (1 - 6 + 3) \\
& \quad + (1/24)\, c_{04}\, (3) \\
& = 1 - .0333 \pm .0192 \\
& \quad + .0288 \pm .0513 \\
& = 1 - .0045 \pm .0547 \, .
\end{aligned}
$$

This represents a downward shift of 0.4 percent, with an uncertainty of 5.5 percent. The 0.4 percent correction could be made by drawing a parallel line to the curve, shifted downward by that fraction, but it seems not worth doing in view of the 5.5 percent uncertainty. For the up/downwind curve the corrections are equally insignificant. Consequently such corrections have not been made during data reduction.

The most significant quantity, for this work, is the ratio of the peak of the distribution to the area under the distribution, as a function of the upwind and crosswind standard deviations. As mentioned before, the quantity, G, in equation (1) above, is a statistical distribution. It is normalized so that the area under the curve is equal to unity, i.e.

$$\text{Area} = 1 = \int_{-\infty}^{\infty}\int_{-\infty}^{\infty} [1/(2\pi\sigma_u\sigma_c)]\, e^{-(X^2+Y^2)/2} \, [H]\, dX\, dY, \quad (5)$$

where the Hermitian peakedness and skewness terms have been abbreviated by the bracket [H].

The power per unit solid angle, I, reflected from a small spot on the water surface that is illuminated by the laser radar beam will have its reflected light spread into a cone where the intensity distribution varies according to the Gram-Charlier distribution. The magnitude of the solid angle of the cone will be taken to be that of the glitter pattern measured simultaneously with the laser return.

Letting I_o be the power per unit solid angle reflected perpendicular to the water surface and hence back to the detector of the laser radar, the

power per unit solid angle in any direction will be given by

$$I = I_o \{2\pi\sigma_u\sigma_c/[H_o]\} G , \qquad (6)$$

where $[H_o] = 1.11$ for peakedness at $X = 0$ and $Y = 0$.

As a verification of the statement in equation (6), note that at $X = 0$ and $Y = 0$,

$$G = G_o = \{1/(2\pi\sigma_u\sigma_c)\} [H_o] .$$

Hence at $X = 0$ and $Y = 0$,

$$I = I_o \{(2\pi\sigma_u\sigma_c)/[H_o]\} \{1/(2\pi g_u\sigma_c)\} [H_o] ,$$

and $I = I_o$, as it should be.

Now the total reflected power is given by

$$P = \int_{-\infty}^{\infty}\int_{-\infty}^{\infty} I \, dX \, dY .$$

Inserting I from equation (6) gives

$$P = \int_{-\infty}^{\infty}\int_{-\infty}^{\infty} I_o \, (2\pi\sigma_u\sigma_c/[H_o]) \, G \, dX \, dY .$$

Then from equation (5)

$$P = I_o \{(2\pi\sigma_u\sigma_c/[H_o]\} . \qquad (7)$$

Now, the total reflected power, P, is the power radiated by the lasar radar in the pencil beam, P_o, multiplied by the Fresnel reflectance of water at normal incidence, r , or

$$P = rP_o = rI_o \{2\pi\sigma_u\sigma_c/[H_o]\} . \qquad (8)$$

Inverting gives

$$I_o = rP_o \, (1/2\pi\sigma_u\sigma_c) \, [H_o] . \qquad (9)$$

The flux at the detector, F_{og}, the power returned per unit area of the detector receiving optics, is given by I_o times the solid angle subtended by a unit area at the detector optics, or

$$F_{og} = I_o \times 1/R^2$$

$$= rP_o \{1/(2\pi\sigma_u\sigma_c)\} [H_o] /R^2 . \qquad (10)$$

c. Fresnel Reflectance of the Sea

Use of the water reflectance for normal incidence in the preceding section perhaps needs some discussion. During the measurement of a glitter pattern the reflection at each glint is at normal incidence. Similarly, for the light scattered back to the laser detector from a pencil laser

radar beam, the angle of incidence is again zero. On the other hand, for the light that does not return to the receiver because it is reflected out into an elliptic cone, the angle of incidence at the reflecting facets is not zero. However, the contribution of scattered light for facets with angles of incidence greater than 2 sigma is negligible. Since the maximum sigma encountered in this work was 7.5 degrees, the variation of reflectance for angles of incidence of this magnitude needs to be examined.

The reflectance of a dielectric surface of index of refraction, n, as given by the Fresnel equations, for light with its electric vector perpendicular to the plane of incidence is

$$r_s = \left| \frac{\cos \Theta - (n^2 - \sin^2 \Theta)^{1/2}}{\cos \Theta + (n_2 - \sin^2 \Theta)^{1/2}} \right|^2 \qquad (11)$$

For light with its electric vector parallel to the plane of incidence, the reflectance is

$$r_p = \left| \frac{-n^2 \cos \Theta + (n^2 - \sin^2 \Theta)^{1/2}}{n^2 \cos \Theta + (n_2 - \sin^2 \Theta)^{1/2}} \right|^2 . \qquad (12)$$

At normal incidence, $\Theta = 0$ and $r_s = r_p = r$.

For unpolarized light at other angles, the total reflectance is

$$r = (r_s^2 + r_p^2)^{1/2}$$

The reflectance, r, at some representative angles, for water of index n = 1.333 (at 16C) is given in Table III.

TABLE III. REFLECTANCE OF WATER AS A FUNCTION OF INCIDENCE ANGLE, Θ

	Θ	r_s	r_p	r	Factor
Normal incidence	0°	.02037	.02037	.02037	1.000
	10°	.02133	.01944	.02038	1.001
	20°	.02449	.01662	.02055	1.009
	30°	.03093	.01194	.02144	1.053
	40°	.04316	.00585	.02450	1.203
	45°	.05299	.00281	.02790	1.370
Brewster's angle	53.1°	.07817	.00000	.07817	3.838
Grazing incidence	90°			1.0	

As can be seen from the above, the total reflectance for unpolarized light varies very slowly with angle of incidence, even up to fairly large angles. The increase in reflectance is only 5% at 30 degrees. This is because r_p falls as r_s rises for angles less than the Brewster angle.

The results of Cox and Munk were also obtained using the same assumption as made here, i.e. that the reflectance of the water surface was cons-

tant and equal to the normal incidence value for all the angles encountered.

d. Lambertian Reflectance

In order to compare calculations of predicted returned power to actual measured values, it is useful to relate glitter reflection to Lambertian reflection, where scattering is completely diffuse, as from a white sheet of paper. However the comparison will be made to a Lambertian type reflecting surface which reflects the same fraction of the total power on it as the reflectance for normal incidence from water, i.e. a fraction .0204 of the incident light is returned, when integrated over all angles within a hemisphere.

In general, for Lambertian reflection, the power per unit solid angle, I_{oL}, returned at perpendicular incidence, is given by

$$I_{oL} = P/\pi \qquad (13)$$

where P is the total power reflected from the surface, integrated over all angles.

In the case of an idealized Lambertian water surface, the reflected power is given by

$$P = rP_o$$

where, as before, r = .0204 for the water surface.

The flux at the detector, the power returned per unit area, would then be given by

$$F_{oL} = rP_o/\pi R^2 \qquad (14)$$

This will be called the "Idealized Lambertian return flux". To summarize, it is the flux returning at normal incidence from a Lambertian surface that reflects, integrated over all angles, a total fraction of the incident light equal to the reflectance of water for normal incidence (.0204).

e. Calibration with Lambertian Reflectance

Calibration of the Lambertian reflectance coefficient for the white paper used as a reference in the field was obtained by measuring the ratio of laser radar return signals from a small segment of area, A_t, of the white paper target, to the return signals for specular reflection from a plate glass window.

The Lambertian reflectance, r_L, of the the white paper is given by

$$r_L = \frac{\pi\, r_s\, P_L\, R_L^4}{4\, A_t\, P_s\, R_s^2}$$

where

where r_s = Reflectance of the plate glass window, for two surfaces = .0826 for n = 1.51,

P_L = Laser signal from a small area Lambertian target,

P_s = Laser signal from a plate glass window,

R_L = Distance to the Lambertian target,

R_s = Distance to the plate glass window, and

A_t = Area of the white Lambertian target, small enough to lie within the central flat illumination region of the laser transmitted beam.

The calibration described above was independent of the Lambertian properties of the calibrating target of white paper. That is, it did not matter if the target did not follow the Lambertian behavior of brightness being proportional to the cosine of the angle from the normal. This was because the calibration technique involved only measurements made with the laser radar and hence with a small acceptance angle near normal incidence.

The flatness of the plate glass window used in the calibration was measured by determining the position of the reflected image of an incandescent lamp source. This permitted calculating the radius of curvature. The glass was then treated as a curved mirror, although this correction was very small.

The value of Lambertian reflectance obtained was 0.73 . This is comparable to values of about 0.75 given in many tables of values for the Lambertian reflectance of white paper.

f. Effective Reflectance

In order to characterize the optical state of the rough water surface, it is useful to define a quantity, ρ_{eff}, the effective reflectance of the water surface, as
in

$$\rho_{eff} = \frac{\text{Return flux from glitter}}{\text{Idealized Lambertian return flux}}$$

$$= \frac{F_{og}}{F_{oL}} \quad . \qquad (15)$$

This quantity can be measured directly in terms of the ratio of laser radar return signals from a water surface to the signals from a Lambertian surface such as a white paper target, often at a different range from that of the water. This is discussed in detail later in this report, but to avoid confusion it should be mentioned here that the ranges of the water and the Lambertian target enter in that case, as well as the actual reflectance of the Lambertian surface used as a reference. In turn, the anticipated sig-

nal from a given model of a laser radar altimeter can be estimated, using a knowledge of the probable range of ρ_{eff} to be expected.

In terms of the model discussed in section A above, an idealized, or predicted, value of ρ_{eff} would be given by equation (15) after substituting expressions (10) and (14),

i.e.

$$\rho_{eff} = \frac{F_{og}}{F_{oL}}$$

or

$$\rho_{eff} = \frac{[H_o]}{2\sigma_u\sigma_c} \quad . \qquad (16)$$

This will be called the idealized ρ_{eff}. The quantity $[H_o]$ is the magnitude of the Hermite polynomial for the two-dimensional Gram-Charlier distribution at normal incidence. $[H_o]$ had the numerical value of 1.11 in all cases encountered here. The quantity ρ_{eff} expresses the optical properties of a rough water surface, in terms of the standard deviations, σ_u and σ_c, of the glitter pattern. It is particularly useful because it does not depend on range and depends only on the optical state of the rough water surface.

The functional relationship expressed by equation (16) made it seem desirable to plot directly measured values of ρ_{eff} as a function of $1/(2\sigma_u\sigma_c)$. The results of such a plot are discussed later in this thesis. The measured values of ρ_{eff} did prove to vary linearly with $1/(2\sigma_u\sigma_c)$.

6. EXPERIMENTAL PROCEDURE

a. Field Site

Experiments to measure laser reflectance as a function of glitter intensity profile were conducted from Parrott's Ferry Bridge over the New Melones reservoir near Columbia, California, following several earlier preliminary experiments at that site and at the Dumbarton bridge over San Francisco Bay. The Parrott's Ferry Bridge was the most favorable of many sites considered as it offered a fairly large distance to the water (109 feet at the time of the last experiments) and had a pedestrian walkway with no obstructions beneath. Heavy automobile traffic and inadequate pedestrian space, as well as obstructions beneath, made such sites as the Golden Gate Bridge and other bridges in the San Francisco Bay area unsuitable. It is hoped that funding for logistic support will be forthcoming so that these experiments can be continued from an aerial platform over open ocean.

The data reported here were all collected at the Parrott's Ferry Bridge on the night of 24 November, 1986, a clear night with no moon present. The wind speed varied from approximately 3 miles per hour to 12 miles per hour. Wind direction varied less than 30 degrees. Due to the short fetch in the reservoir, varying from 1/4 mile to 1 mile, depending on the direction, only high frequency waves and ripples were observed. It is anticipated that results with these waves will scale up to ocean waves observed from higher altitudes.

b. Laser Radar Altimeter Measurements

The laser system consisted of a 0.905 micrometer gallium arsenide diode laser driven by a pulser having a pulse width of 160 nanoseconds at half height. The transmitter output beam divergence was 1.4 degrees by 2.8 degrees. A silicon avalanche photodiode detector with an 8 mm focal length lens was used to receive the reflected laser signal. The aperture field of view was circular with a divergence angle of 3.6 degrees, totally encompassing the area illuminated by the transmitter. A 10 nanometer bandwidth multilayer film filter was included in the detector optics to eliminate noise due to sunlight, for daylight operation. The laser system was mounted on an arm extending 3 feet from the bridge railing. There were no bridge supports or obstructions near enough to produce unwanted reflections. The laser was 109 feet above the water.

The detector output was continuously displayed on a portable oscilloscope. Because the pulse length of the returned laser pulses was about a microsecond, it was necessary to stretch the received pulses electronically and assemble them to form a continuous-wave analog signal to permit recording. By the Nyquist theorem, the maximum component frequency of this signal is limited to 500 Hertz by the interpulse interval of one millisecond. It was thus possible to record this signal on a frequency-modulated analog tape recorder, a Hewlett-Packard HP-3960A recorder, which had a signal bandwidth of dc to 20 kilohertz. The signals were recorded simultaneously with recording of the video pictures of the glitter pattern. Synchronization of the video recordings and laser return signal recordings was accomplished by recording the same voice track on both recorders.

The laser return signal magnitude was later data-processed in the laboratory with a DATA Precision Corp. DATA- 6000 waveform analyzer to yield a mean laser return signal. As the laser return signals were played back from the recorder into the analyzer, 16 sequential waveforms, each consisting of 512 data points taken at 1 msec intervals, were averaged. This process was repeated 5 times for each run and these were averaged to obtain a mean value. Successive averagings of slightly different regions within the ten seconds over which the video signals were averaged yielded a standard deviation for the magnitude of the mean signal.

c. Laser Reference Measurements

An effective Lambertian water reflectance signal was obtained by means of measurements of the laser return signal from a white sheet of paper. These measurements were made in the field shortly after the measurements of water reflectance signal. The white paper sheet was located at a distance of 39 feet. At this distance the transmitted laser pattern was still fully within the boundaries of the sheet of paper. The same paper was separately calibrated in the laboratory and found to reflect 0.73 times as much light at normal incidence as a perfect Lambertian surface. This value is representative of most white paper surfaces. The effective Lambertian water return signal was then obtained by multiplying the signal from the white sheet of paper at 39 feet by the ratios

$$(.0204/0.73) \times (39/109)^2 .$$

The factor (.0204/0.73) takes account of the difference in reflectance of the white paper sheet and the idealized Lambertian water surface. The factor $(39/109)^2$ takes account of the different distances of the white sheet and the water, 39 and 109 feet respectively. The inverse square law applies to these distances.

The effective reflectance coefficient, ρ_{eff}, as defined earlier in section II E, was then calculated by dividing the mean laser water return signal by the effective Lambertian water return signal. i.e

$$\rho_{eff} = \frac{\text{Mean laser return signal}}{\text{Effective Lambertian water return signal}} .$$

d. Glitter Pattern Measurements

Glitter patterns were produced by illuminating the water surface with a quartz-halogen lamp of a type used as a light source in overhead classroom projectors. This produced a nearly uniformly illuminated patch on the water with a total beam angular divergence of about 60 degrees, considerably wider than any of the observed glitter patterns. The uniformity of the illumination was verified in the laboratory in advance. The lamp was rated at 360 watts at 54 volts. Power for this lamp was provided by a small rotary converter generating nominal 120 volts, 60 Hertz power up to 500 watts, and driven by 12 volts dc from an automobile-type storage battery. The lamp voltage was varied, as needed, by means of a variac. The video camera was an RCA type TC2055C with a Vidicon tube. It was operated on 12 volts dc directly from a second automobile storage battery. The camera performance was very stable as it generated its own line-scan frequency with a quartz oscillator. The HP3960A FM data recorder for the laser radar signals also operated with 120 volt 60 Hertz power, obtained from this same battery through a frequency controlled square wave chopper converter. The video images from the RCA camera were recorded on a portable 8mm video tape recorder that was part of an Olympus VX-801-KU 8mm video camera system. This system also displayed a continuous monitor image of the scene as viewed by the RCA camera. This allowed the brightness level of the illumination to be adjusted for proper recording and also permitted alignment of the camera with the major or minor axis of the elliptic glitter pattern. The 8 mm tape system was very compact and operated on its own internal batteries. As measured in the laboratory, the resolution of this combined system exceeded that of the usual home VHS format by about 20%.

The lamp and video camera were mounted on an arm extending from the bridge railing at a point about 6 feet from the laser altimeter. The video camera was oriented first along, then across, the wind direction, so that sequentially the major and then the minor axis of the elliptical glitter pattern would be aligned horizontally in the recorded video image. The 16 mm camera lens was focused at infinity with an aperture setting of f/1.6 . The 16 mm focal length gave a wide enough field of view to include the complete glitter pattern in every case. Recording sequences of 15 to 30 seconds were made at several different illumination levels in order to be sure to avoid saturating the camera.

Later, in the laboratory, the 8 mm video tape recordings were copied into a Sony Superbeta VCR which had more flexible reproducing features than the 8 mm field unit. The resolution of this VCR was previously measured and found to exceed that of the usual home VHS format by 50%. No detectable degradation occurred in this copying process.

The output of the video recorder was sent to a Tektronix 468 digital oscilloscope. Successive single horizontal TV scan lines, lying along, or perpendicular to, the glitter pattern major axis, were displayed on the scope using the "B sweep delayed" mode. The waveform displayed was a time-varying signal proportional to the intensity distribution along the major or minor glitter pattern elliptic axis. The oscilloscope was then set up to digitize and average 256 such sweeps and to store the accumulated waveform. The real time period represented by the 256 sweeps was 256/30 or 8.5 seconds. The computer program in appendix A was written to allow the Tektronix 468 to interface with an IBM PC/XT through an IEEE488 interface bus [Ref. 7]. With the computer as controller for the operation, the oscilloscope digitized and transmitted the waveform data to the computer. The digital information was then stored in memory or on disk for further processing.

The Tektronix oscilloscope was then adjusted so that it displayed a TV line through an image of the prevailing water surface outside the glitter pattern. Sweep averaging and transmission of a waveform to the computer memory were again carried out. This provided a background signal which was subtracted from the glitter waveform in the computer. The computer was then programmed to plot the glitter pattern profile on an Epson FX80 dot matrix printer. Figures 4a and 4b show the resultant intensity profiles along the major and minor elliptic axes from a representative run. Gram-Charlier standard deviation values σ_u and σ_c were then measured graphically from these profiles by measuring the half width at a height equal to 0.659/1.11 times the peak value, as discussed earlier.

7. Results

The measured values of ρ_{eff}, the ratio of observed laser radar return to that expected for Lambertian reflection, were plotted as a function of the corresponding values of $1/(2\sigma_u\sigma_c)$, in Figure 5, (see section IV) where σ_u and σ_c were the measured upwind and crosswind Gram-Charlier standard deviation values for the glitter patterns. The data values are tabulated in Table III.

Use of the function $1/(2\sigma_u\sigma_c)$ for the abscissa was suggested by the model discussed in section 5 of this appendix. This functional form organized the experimental points so as to fall fairly well along a straight line. The solid straight line was a least squares solution for the data points taken here, shown as the circles in that figure. The correlation coefficient was r = 0.96 for the points relative to this line. This line had a slope of 0.92 and an intercept of 44 on the ordinate axis.

This empirical relationship provided a basis on which to predict the expected reflectance of a pencil beam from a rough water surface on the basis of only the remote sensing measurement of the glitter pattern profile. This made possible the field evaluation of working models of laser radar altimeters with the help of a simple technique. The functional rela-

TABLE IV

Run #	Glitter Profile Standard Deviations: Upwind (σ_u)	Glitter Profile Standard Deviations: Crosswind (σ_c)	Effective Laser Reflectance (ρ_{eff}): Predicted	Effective Laser Reflectance (ρ_{eff}): Observed	Inferred Wind Speed
1	.340	.094	17.4	46.8	13.7
2	.224	.121	20.5	47.6	7.18
3	.175	.141	22.5	42.0	5.60
4	.134	.058	71.4	90.5	2.41
5	.122	.026	175	150	1.72
6	.163	.024	142	182	2.90
7	.081	.030	228	213	1.07
8	.084	.034	194	217	0.92
9	.218	.064	39.8	89.8	5.69
10	.181	.058	52.9	92.7	4.04
11	.241	.120	19.2	73.0	8.45
12	.135	.118	34.8	88.3	4.80
13	.167	.110	30.2	72.3	4.43
14	.150	.100	37.0	86.9	3.58
15	.126	.046	95.8	116	2.39
16	.217	.201	12.7	43.5	10.4
17	.301	.096	19.2	42.3	11.0

tionship, and also the body of data were the first of this sort in this field. Without this technique, the field performance of a given laser altimeter system would require expensive concurrent logistic support to determine the roughness state of the water. The latter was likely to be inferred from meteorological and oceanographic data, and to be only the deduced probable steady state condition, whereas the technique reported here directly measured the momentary optical state of the ocean surface.

The numerical values of ρ_{eff} were of immediate utility. The lowest value, represented by the intercept on the y axis, was 44. Although extrapolation to the axis had considerable uncertainty, it did imply that for the worst case the ratio of reflectance to that for Lambertian was considerably above unity, at least by somewhat over one order of magnitude. Without evidence such as this, a working altimeter would presumably have had to be designed to cope with a case where a unity ratio to Lambertian might have occurred. This factor of 44, or somewhat over one order of magnitude increase in signal, represented a large reduction in the design requirement to be sure of a return signal. This had immediate importance in the ability to achieve the design requirements.

That the observed signals were directly relatable to reflection from a Lambertian surface, made it possible to do most of the testing work in the laboratory. Various evolutions of laser radars could be tested with a Lambertian surface such as a white sheet of paper. The signals could then be scaled to those for a water surface at any required distance. The range of field signal return values could then be evaluated in terms of Figure 5 (section IV)

The model proposed in Section 5 (of this Appendix), which predicted that

$$\rho_{eff} = [H_o]/(2\sigma_u\sigma_c),$$

required a straight line through the origin with slope $[H_o] = 1.11$ in Figure 5. This is represented by the dashed line in that Figure. The existence of a theoretical model that agreed with the observed behavior in more detail would have been desirable, but it was not necessary. The present experiment had achieved the stated objective of providing a means of determining the optical state of the rough water by a remote sensing technique, where none existed before this work. The result was semiempirical, but was useful.

The fact that the proposed model did not predict the observed behavior could be viewed as an interesting challenge. That the observed effective reflectance was larger than expected, by somewhat less than a factor of four, and that the straight line had an intercept, indicated that this was a problem unlikely to be related to miscellaneous small increases or losses of light. Some of the immediate, ad hoc, explanations of this discrepancy that come to mind, seemed to predict less reflectance, rather than more. For example, if the variation of specular reflectance with angle were invoked for light reflected at large angle of incidence into the far wings of the Gram-Charlier distribution, then less light should have returned along the axis, rather than more.

Another effect producing deviation toward too little reflection, was that the laser "pencil" beam had a finite divergence of 1.4 by 2.8 degrees. Thus the reflectance was really the average over the curved top of the Gram-Charlier distribution. Thus the average observed would have been sliightly less than the peak value. Correction for this is planned in subsequent work, but this correction will produce an increase in the peak reflectance, rather than a decrease, as needed to fit the model.

A possibility, in the right direction, in that it would have tended to produce the higher than expected values of reflectance was that some spray might have developed as the wind increased. This corresponds to the region of small values of $1/(2\sigma_\mu\sigma_c)$. The droplets would have acted as retroreflectors and increased the returned signal along, or near, the laser beam axis. This effect, called the "glory" is commonly seen in looking down from an aircraft in the direction of the shadow of the aircraft. However, this explanation seems quite unlikely in view of the low sea state encountered on the reservoir.

8. COMPARISON WITH OTHER RESULTS

Direct comparison of the results reported here with those of others was possible only for one bit of fragmentary data. No other measurements of laser reflectance as a function of glitter pattern width were known to the author, except for a single diagram in the article by Petri [Ref. 2]. The values of glitter pattern width were not quoted there, as the article was primarily concerned with measuring the peak reflectance as a function of wind velocity. However, a few sample glitter pattern profiles were shown in one figure. That figure is reproduced here as Figure 9. It was possible to measure the sigma values graphically from these curves, although the curve shapes were poor. Those curves were obtained by a laser scanning in a vertical plane, with the plane rotating slowly through 360 degrees about a vertical axis. The scans were averaged so that no information was retained on the relative magnitude of upwind and crosswind sigma values. Two of these curves yielded sigma values that could be related to the results in this thesis. The others were too poorly resolved or they corresponded to reflectivity above or below the range measured in this work. Two pairs of these curves were for essentially the same windspeed so that an estimate of the internal consistency could be made. These pairs differed by 12% and 14% for the peak value. Points for the two utilizable widths were plotted with the symbol + on Figure 5 (section IV). They fell close to the data points obtained in this work.

Although the results obtained in the work reported here were intended to provide a means of evaluating laser radar altimeter performance without the necessity of knowing the wind speed, it was interesting to relate these results to data taken by others, where the wind speed was measured. This provided some confirmation of the validity of the results reported here.

An indirect comparison, where an inferred wind speed allowed intercomparison with related experimental data in the literature, was possible by

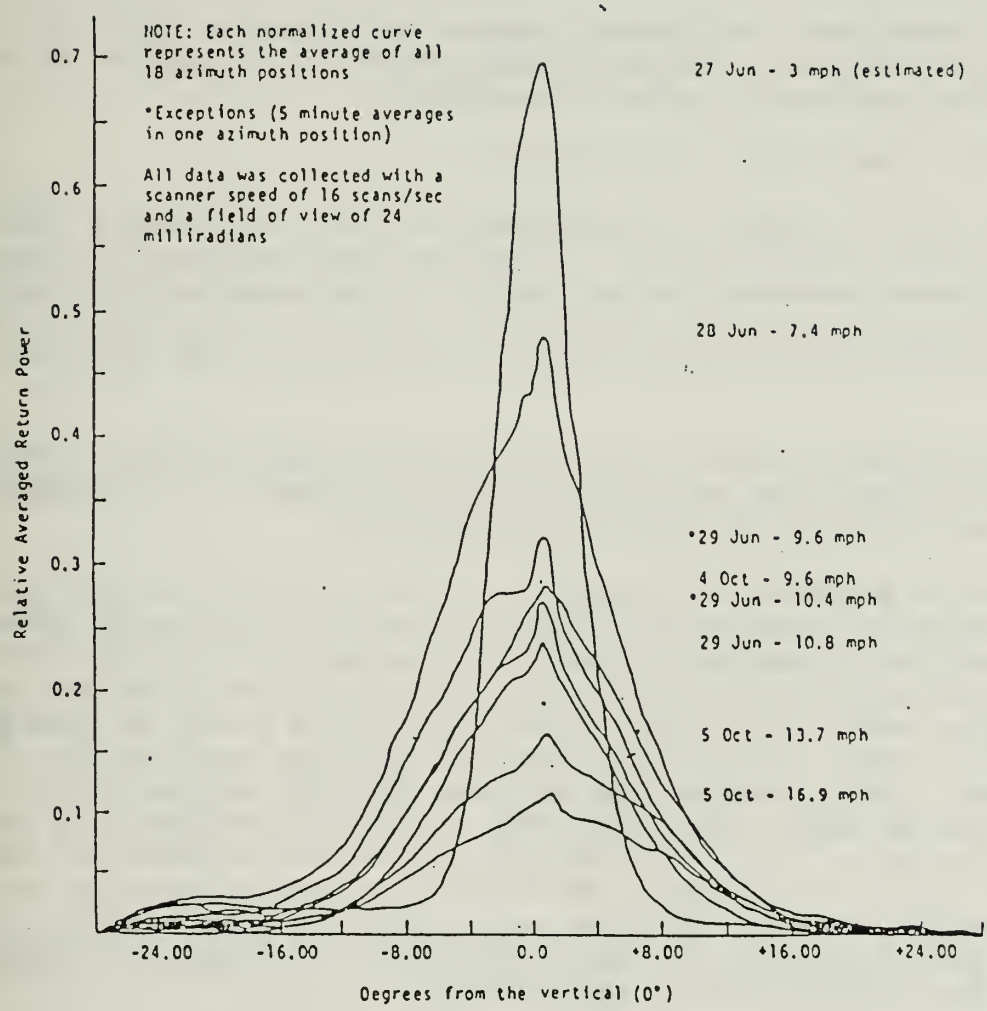

Figure 9. Normalized average return signal versus laser/receiver angle as reported by Petri [Ref. 2].

combining the results of Petri [Ref. 2] with the results of Cox and Munk [REF. 3]. Petri reported laser reflectance data in terms of wind speed for waves under the Chesapeake Bay bridge near Annapolis, Md. Figure 10 reproduces the results of Petri for laser return as a function of wind speed, with his results plotted as the crosses. No theoretical model was offered in that article.

Cox and Munk gave a relationship between their measured wind speed and the mean square upwind and crosswind sigma values for the glitter patterns, where W was the wind speed in meters per second, as

$$\sigma_c^2 + \sigma_u^2 = .003 + 5.12 \times 10^{-3} W \pm .004 \ .$$

W has been called the effective wind speed here, as it was only a means to cross-connect to the data of Petri. Using the above expression, effective wind speeds were calculated for our data. The corresponding laser returns are plotted as the circles in Figure 10. It can be seen that the data points from both sources cluster into a broad band in the same general region.

The approximate agreement of the data reported here with the combined results of Petri and Cox and Munk gave some credence to the ability to relate laser radar return to the width of glitter patterns.

It should be pointed out again that the purpose of this work was to obtain a measure of expected laser radar return signal from rough water by remote sensing techniques and without a knowledge of wind speed. The effective wind speed deduced from the expression of Cox and Munk was useful for correlation with Petri's data. These wind speeds should be considered here only as a means of obtaining order of magnitude confirmation of the optical results. Intercomparison was somewhat doubtful because the Cox and Munk data were for open ocean waves, with wind speeds measured at 9 and 41 feet above the water. The Petri results were for waves under the Chesapeake Bay bridge near Annapolis, Md, with wind speed measured at 60 feet above the water. In spite of these uncertainties in wind velocity it was interesting that utilization of these results yielded approximate agreement between the data reported here and that of Petri.

9. CONCLUSION

This work showed the feasibility of a remote sensing technique for determining the expected magnitude of laser radar return from a rough water surface by measurement of the size of a simultaneously measured elliptical glitter pattern. The technique did not require any additional knowledge of the water surface beyond optical measurements made at the location of the laser radar altimeter. To the authors' knowledge such a technique was not available previously. The effective laser reflectance, ρ_{eff}, proved to vary approximately linearly with $1/(2\sigma_u\sigma_c)$, where σ_u and σ_c are the Gram-Charlier standard deviations for the upwind and crosswind glitter pattern intensity profiles, respectively. ρ_{eff} is the ratio of the laser radar return signal to the laser radar return signal to be expected from the water if it were to act as a Lambertian, diffuse reflecting, surface but with an overall reflectance coefficient equal to that for normal incidence for water. A least squares fit to a straight line gave a slope of 0.92 and a y intercept of 44, with a correlation factor, r = 0.96 .

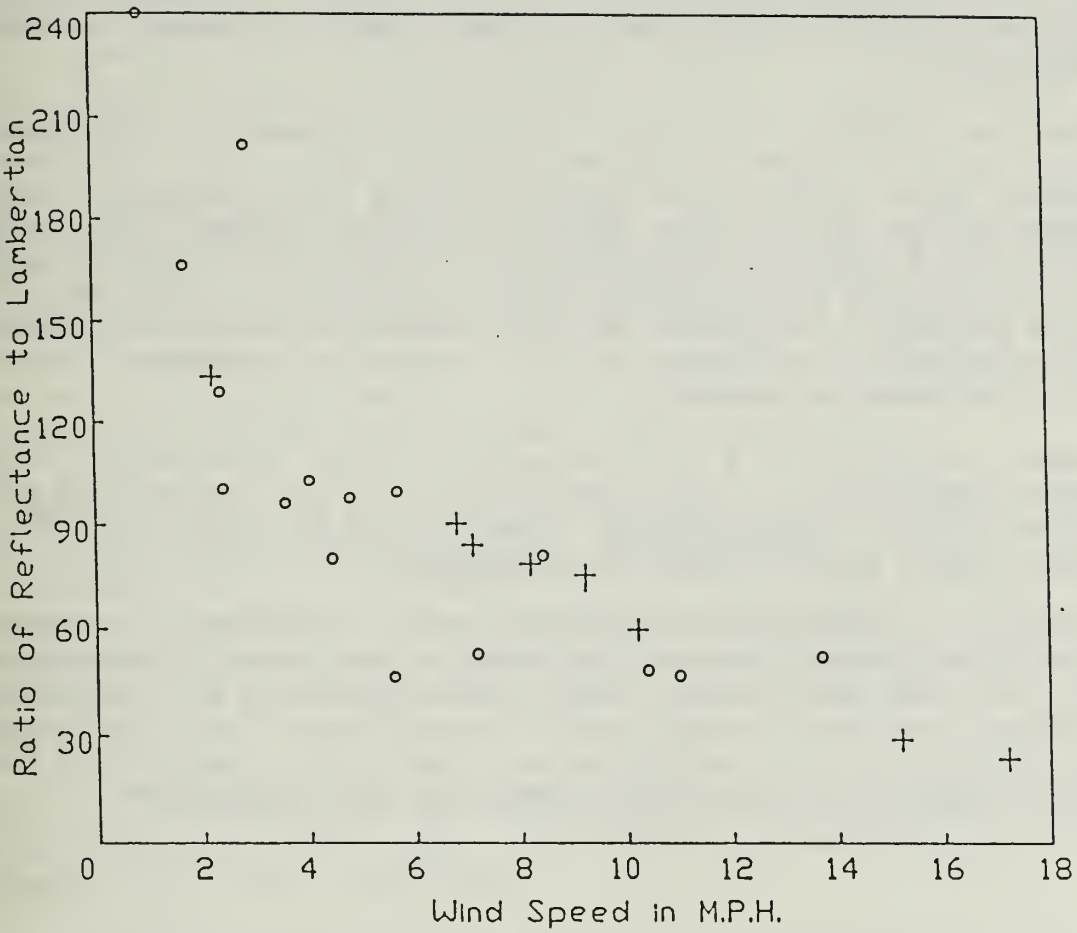

Figure 10. Plot of observed effective reflectance relative to Lambertian, ρ_{eff}, versus wind speed. Circles represent reflectance data obtained in this work plotted versus inferred wind speed. Crosses represent reflectance data collected by Petri plotted versus measured wind speed [Ref. 2].

Plotting ρ_{eff} as a function of $1/(2\tau_u \tau_c)$ was suggested by the model proposed in this report. That model indicated that a straight line for ρ_{eff} as a function of $1/(2\tau_u \tau_c)$ should pass through the origin with a slope of $[H_o]/4$, or perhaps a slope of $[H_o]$, where $[H_o] = 1.11$, under a different, controversial, interpretation. The solution to the discrepancy between the observed data and the suggested model is a problem that remains for further work.

That the straight line did not go through the origin, but instead had an intercept of 44, provided important information. This said that the worst case of very rough water should provide a return signal 44 times the magnitude of that from a water Lambertian surface. Although such extrapolation to zero is risky, it implied that for very rough water the smallest laser radar return is somewhat more than one order of magnitude larger than would be assumed in the absence of this information. This would permit the design of a laser radar altimeter with an order of magnitude less power than would otherwise be necessary.

These results provide a relationship between the reflectance of a rough sea surface and that of a Lambertian surface, such as a large white surface at limited range in the laboratory. This reduces the need for field tests of various working models of laser radar altimeters.

It should be pointed out that these results are tentative because they have not been tested on actual open ocean waves. Work is in progress to utilize more nearly ocean waves, using measurements made from the middle of the Golden Gate bridge. It is planned to extend these measurements to open ocean with the use of a helicopter as a platform. The present results should be considered tentative until the open ocean work is completed.

APPENDIX B, READOUT CIRCUITS, CALIBRATION AND ADJUSTMENT

1. Operation of the Readout Package

The circuit diagram of the readout package is shown in Fig. 11. The simplest description of the entire readout circuit results from first explaining the operation of the sample-and-hold circuit (S & H) which is chip M, and the instrumentation amplifier, which is chip N. These comprise the last two stages of the circuit.

Fig. 12 shows the voltage waveforms which relate to the sample-and-hold circuit. Waveform (a) represents the firing of the laser. Waveform (b) is the return trigger. It is derived from the leading edge of the return signal; because of inherent delays in the circuitry it is delayed in time relative to the actual reception of the return signal radiation. Ideally this is a constant time delay. A detailed description of the return trigger will be given in the section entitled "leading edge detector".

The logic waveform (c) goes high approximately 3 μsec prior to laser firing. It goes low at the time of the return trigger. In the case of no return trigger, the dotted waveform (c) is formed for the logic into the S & H and the dotted waveform in (e) gives the corresponding S & H output. The logic waveform originates in chip H, a retriggerable monostable multivibrator. A detailed description of this will be given in a later section.

Waveform (d), the ramp input to the S&H has a fixed positive bias of 0.12V. It rises to about 3.0 V in 2 μsec. It's start relative to the laser firing is adjustable with the "zero time adjust".

Referring to waveforms (c), (d), (e) we see that when the logic is low, S&H is in the hold mode; when the logic is high S&H is in the sample mode. Thus the logic in (c) for the solid line yields the solid line for the held voltage in (e) corresponding to the time of the return trigger. When there is no return trigger the logic in (c), dotted line, yields the dotted line waveform and the held voltage is 0.12V corresponding to the positive bias of the ramp input. In waveform (e) note the previously held voltage which drops to 0.12V at the start of the sample mode.

The output of S&H, i.e. waveform (e), is inputted to the instrumentation amplifier, chip N. Chip N amplifies the S&H output; it also can be biased by an adjustable amount. In our case, it is biased by an amount which just cancels the input bias of 0.12V. This is done by regulating the "bias adjust" until the altitude readout voltage is zero, when there is NO return trigger.

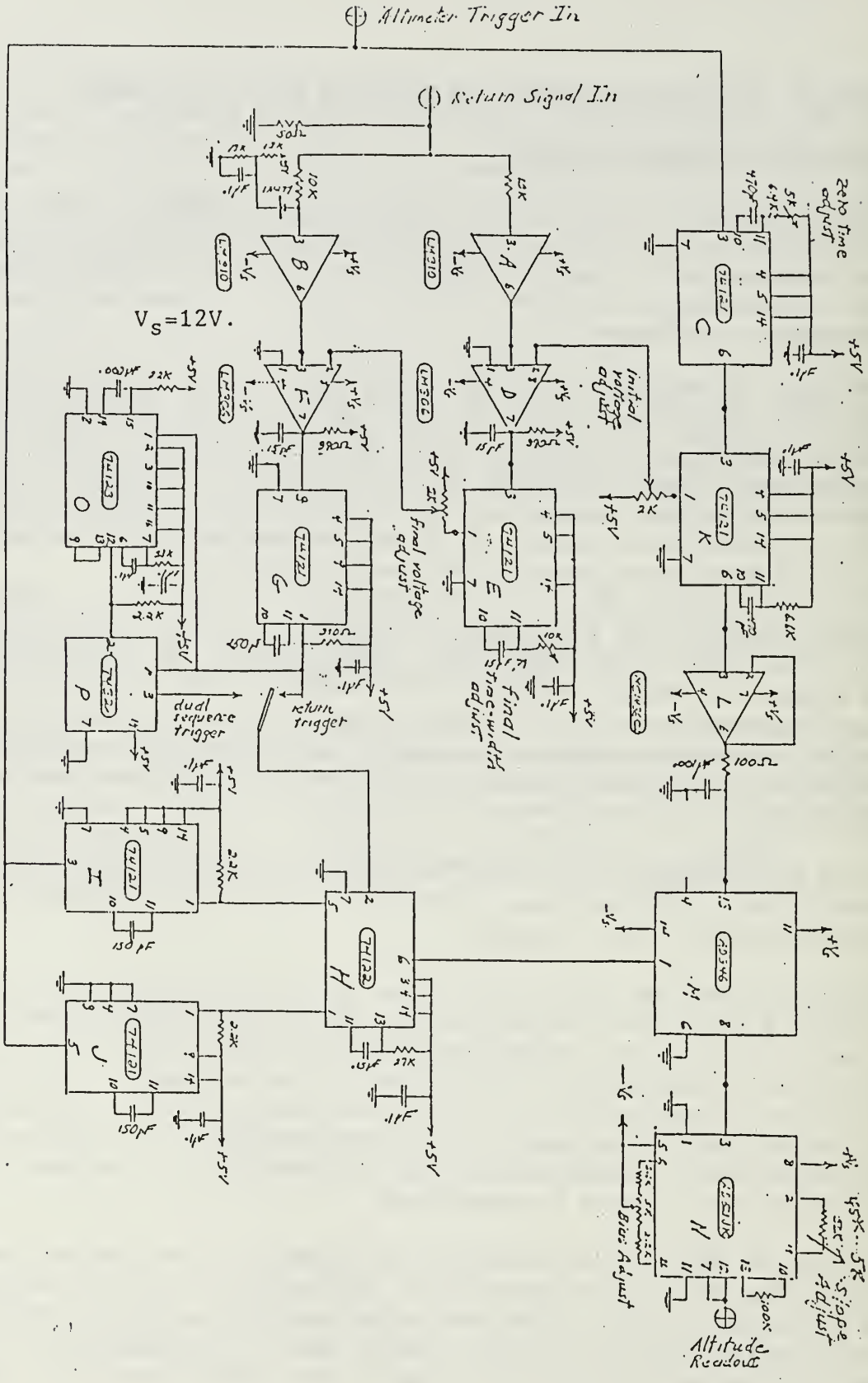

Figure 11. Altimeter readout circuit

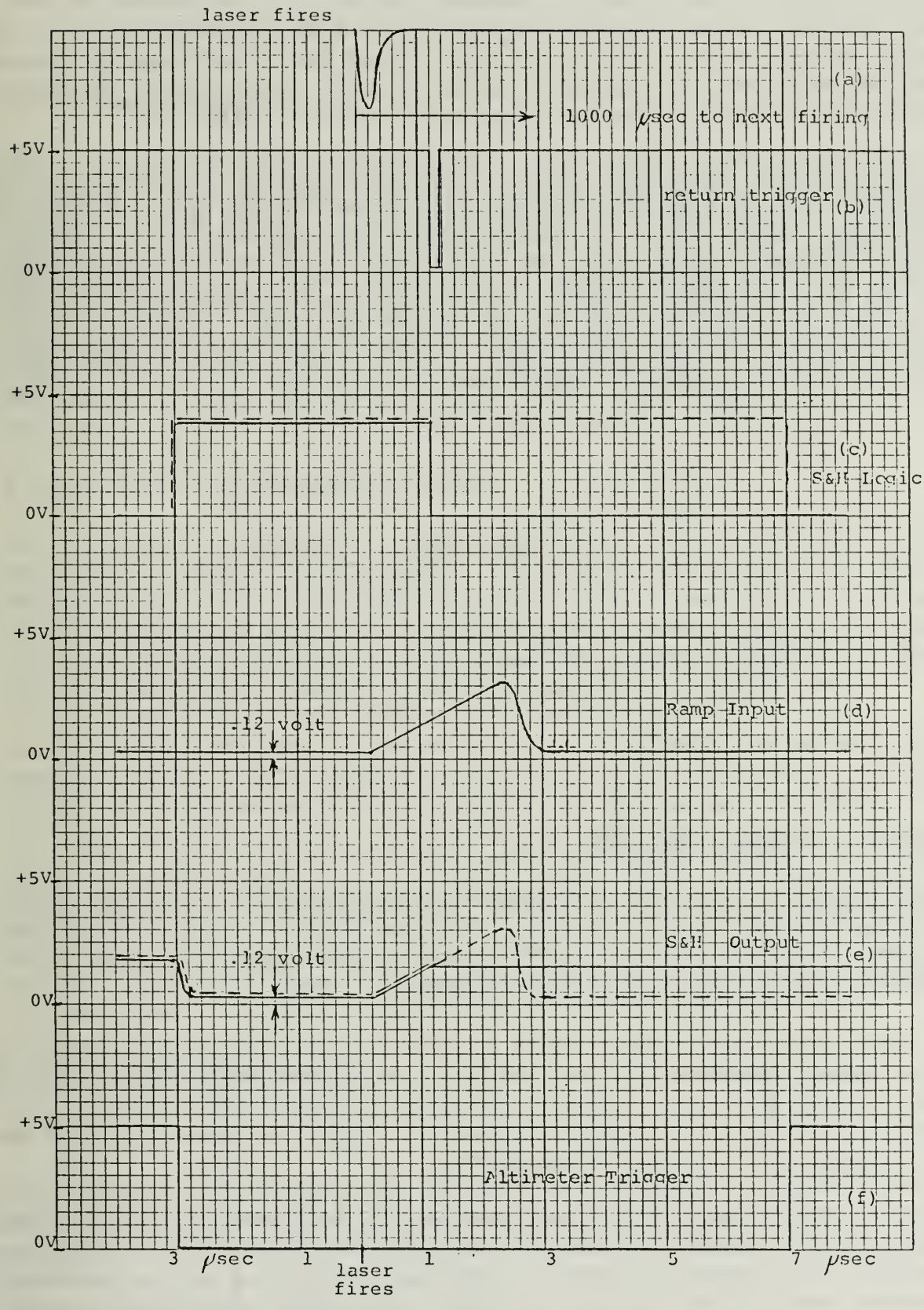

Figure 12. Sample and hold voltage waveforms

The gain of chip N can be set by choosing the value of the resistor between pins 2 and 14. In our case it has been chosen so that when the return trigger changes from a time near laser firing to a time exactly 2 usec later, the output of N changes by exactly 6 volts. Thus chip N, in effect, converts the S&H into the ideal case described in the first section.

Fig. 13 shows the properly biased ideal altimeter readout waveform, i.e. at the output of N, for the case where the ramp portion starts at the time of laser firing. Assume that the return trigger corresponds to zero altitude. The time delay shown is thus due to all of the inherent circuit delays leading up to the return trigger. Obviously if we correspondingly delay the start of the ramp to coincide with the return trigger shown in Fig. 13, the output will be properly zeroed. This is done by using the "zero adjust". Preferable methods for zeroing are discussed later.

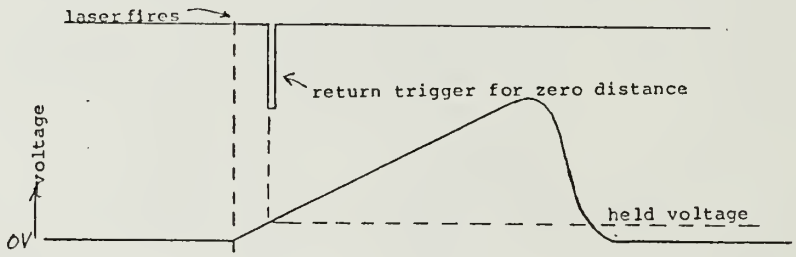

Figure 13. Inputs to the readout package from the altimeter package

2. Inputs to the readout package

In the previous section we attempted to explain the vital workings of the altimeter readout without being too detailed. Now we will describe the complete readout circuit. First we will mention the two inputs to the readout package from the laser altimeter package.

The return signal input (BNC input) is the output of the detector amplifier in the laser altimeter. It is a positive waveform which rises to peak value in about 0.15 usec and which saturates at about 6.5V amplitude. It's total length is about 0.6 usec. The return trigger is generated from the return signal in the "leading edge detector".

The altimeter trigger (BNC input) goes low about 3 usec before laser firing and stays low about 10 usec. See Fig. 12f. It originates in the laser circuitry of the laser altimeter. The beginning time of the altimeter trigger is used in the altimeter readout for generating the ramp waveform and in the "leading edge detector". Both beginning and end times of the altimeter trigger together with the return trigger are used to generate the logic waveform.

3. The ramp generator

Chip C is a monostable multivibrator. Its output goes positive at the beginning of the altimeter trigger. The time length of this positive pulse is about 3 μsec and is adjustable with the "zero time adjust". The pin 6 output then inputs chip K which outputs at pin 6 a 2 μsec wide positive pulse delayed by an amount equal to the variable pulse length of chip C's output. This waveform then inputs the specially selected op-amp follower, chip L (MC1436CU) which has a slew rate of about 1.5V/usec resulting in a ramp waveform output about 3V high. Since the input is biased to 0.12V, the output also has that bias. The RC network load helps to linearize the ramp output which is then fed into the S&H circuit, i.e. chip M.

4. Logic input to the sample and hold

Three triggers are required to form the logic input to the S&H. One is the return trigger (See Fig. 11f). The other two are derived from the beginning and end of the altimeter trigger. The beginning of the altimeter trigger immediately triggers chip I whose output, the pre-trigger, goes low for about 150 ns. The end of the altimeter trigger immediately triggers chip J whose output, the post-trigger, goes low for about 150 ns.

These three triggers are inputted to H, a retriggerable monostable multivibrator (74122). Its output is the logic input to the S&H. The return trigger is connected to H so as to turn H on. The nominal on-period of H is purposely made longer than the 1000 μsec period between laser pulses. When the post-trigger appears a few μsec after the return trigger, H is retriggered and still remains on; then almost 1000 usec later, the pre-trigger resets H (i.e. turns it off). Without a return signal, H is not turned on until the post-trigger appears. It then remains on until the next pre-trigger. (Note that H on, corresponds to low output and H off corresponds to high output.) Refer to Fig. 11c for the logic waveforms.

5. The leading edge detector

a. Summary

The purpose of the leading-edge-detector is to produce a trigger (from high to low) which is generated by the steep part of the leading edge of return signals which are above an arbitrarily chosen amplitude. This is accomplished by using two voltage comparators acting in tandem. The first comparator establishes a reference time at which the return signal exceeds a one volt threshold. This then generates a second threshold of about 2.5 volts which occurs in a time window of 50 ns whose start is delayed by 80 ns from the reference time. The return signal together with the second threshold, input the second comparator. If the return signal exceeds this threshold during the 50 ns time window, the second comparator fires. It feeds a monostable multivibrator whose output is a high to low pulse of 150 ns width. This is the return trigger which we have referred to previously.

b. Detailed description

For a more detailed description we refer to Figs. 11 and 14. The return signal inputs two identical op-amp followers, i.e. chips A and B. These serve to isolate the inputs to the two comparators D and F. The network preceding the input of B limits the input and output of B to about 4.9 volts.

Fig 14a shows the first threshold and this is inputted to the comparator D. This is a gated waveform which has the same timing as the positive pulse which generates the ramp. (See the section on the Ramp Generator.) The one volt level is set using the "initial voltage adjust". Although the start of this waveform is adjustable (as described in the second section) it precedes any return signals. The waveform lasts for 2 μsec, long enough to accommodate return signals from an altitude of 300 meters. This comparator fires (output goes low) for return signals which exceed the 1 volt threshold and the output triggers the monostable multivibrator E. The width of the output of E is adjusted by the "final time-width adjust", and the threshold adjusted by the "final voltage adjust". This output constitutes the timed threshold for the second comparator F. The waveform is shown in Fig. 13b. It is delayed by about 80 ns from the time the first comparator D starts to fire.

Fig. 14b shows a portion of Fig. 14a with expanded voltage and time scales. The solid curve for return signal corresponds to that in Fig. 14a. The dotted curve for return signal is for a lower amplitude which is the minimum amplitude to just fire the second comparator. The solid and dotted threshold curves are for the corresponding return signals. What is significant here is the time difference when F starts to fire for the two cases shown. This difference is 140-100=40 ns. This corresponds to a difference in the altimeter readout of 6 meters. Measurements with the readout test pulser (which simulates the return signal-see Readout Test Pulser), yield about a total difference of 7 meters in the readout between a return signal of 3 volts amplitude and a large return signal of 6 volts amplitude. A large part of this output variation with return signal amplitude is due to the return pulses which just exceed the minimum of 3 volts amplitude.

The output of the second comparator F (Fig. 11) is delayed relative to the times indicated on Fig. 14b. Similarly the output of G, which is the nominal return trigger, is further delayed. These delays are for the most part constant and therefore compensated by use of the "zero time adjust".

c. Dual sequence trigger

Field tests using horizontal ranging have utilized the above nominal return trigger. An optional addition to the leading-edge detector (Fig. 11) is the dual sequence trigger circuit. Its input is the nominal return trigger and it's output replaces the nominal return trigger to input chip H, the

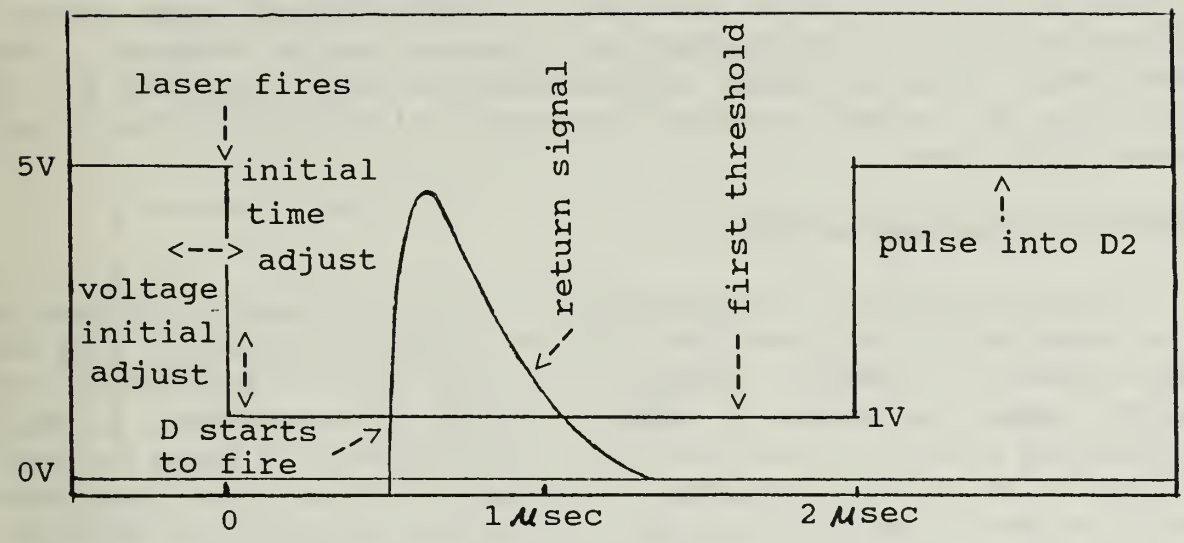

(a)

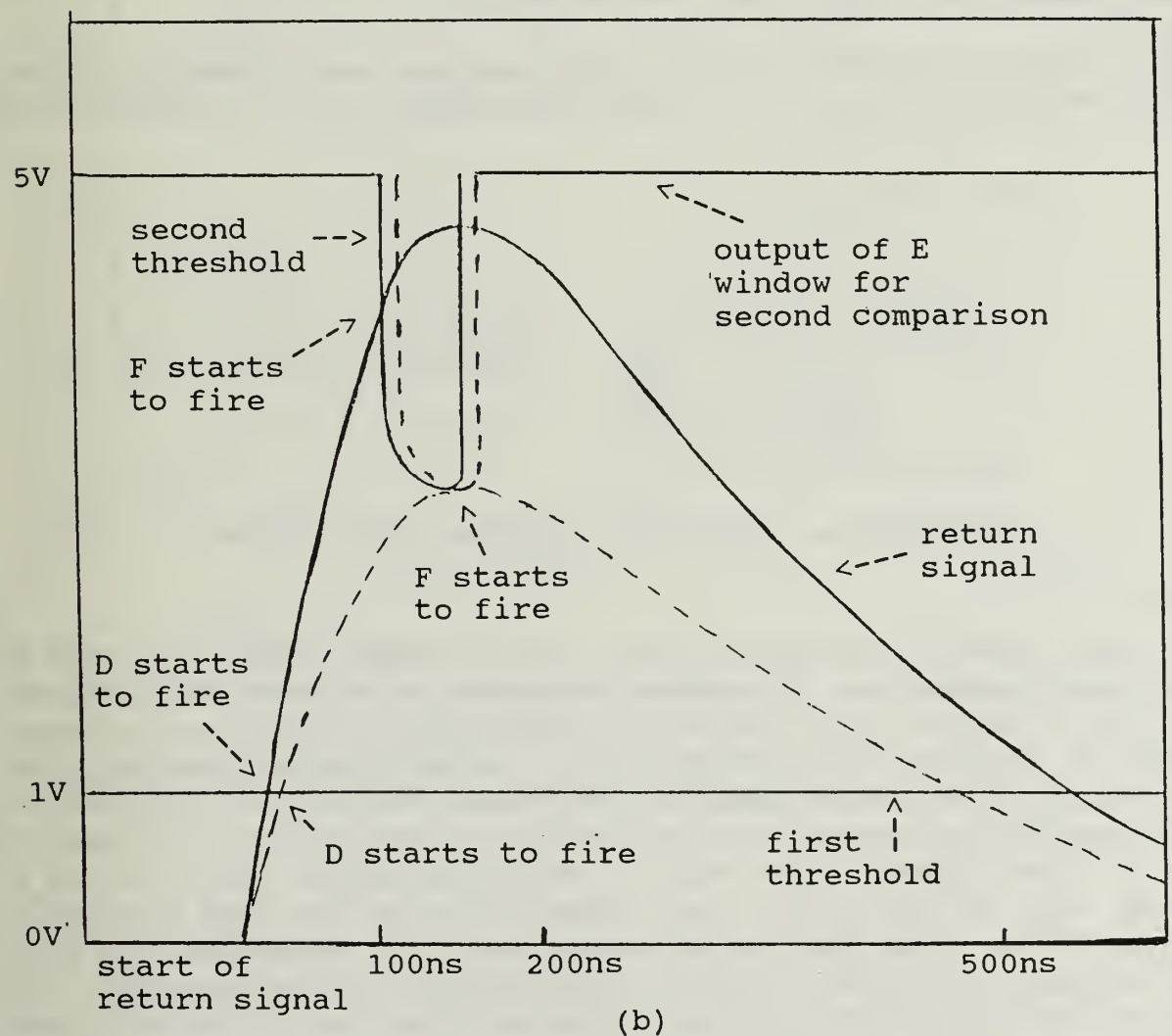

(b)

Figure 14. Waveforms at the comparator

retriggerable monostable multivibrator. This circuit outputs a trigger only whenever there are two nominal return triggers in direct sequence, i.e. 1000 usec apart. Thus if there are no missing nominal return triggers this circuit will have no missing dual sequence output triggers. This circuit can be used to reduce the possibility of false triggering due to solar noise. It has been successfully tested in the lab using controlled amounts of light noise.

d. Improved leading-edge detector

The leading-edge detector described above in parts 5,a,b,and c was used in recent successful field tests for the laser altimeter together with the readout package. However, subsequent to these tests, a modification has been lab tested and appears to offer a significant improvement. Firstly measurements with the readout test pulse indicate about a 3 meter variation in altimeter readout corresponding to a range of return signal amplitudes from 3V to over 6 volts, whereas the original version had a 7 meter variation. Secondly it has been successfully used for extensive lab tests for false triggering due to light noise. (See section V.)

Fig. 15 shows the modified circuitry which has been used. The RC differentiator results in an input to B which approximates the first derivative of

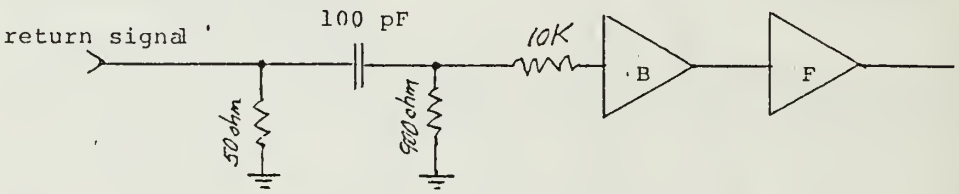

Figure 15. Improved "leading edge" circuit

the return signal. This differentiated signal is then used as the input to the second comparator. It replaces the return signal input used originally. Fig. 16 shows the 3V amplitude return signal which was also shown dotted in Fig. 14b. Also shown is the corresponding differential pulse. The window for the second comparator F is timed the same as in Fig. 14b but it's threshold is lowered so as to just fire for the differential pulse of the 3V return signal. Note that the second comparator starts to fire at 115 ns while for the larger return signal (shown in Fig. 14b) it starts to fire at 100 ns. Thus the time difference here is 15 ns compared to 40 ns for the case in Fig. 14b, a marked improvement in timing accuracy. The reason for the improvement lies in the fact that the differential peak occurs sooner in time than the peak of the return signal, resulting in less time variation for return signals close to the 3 volt minimum.

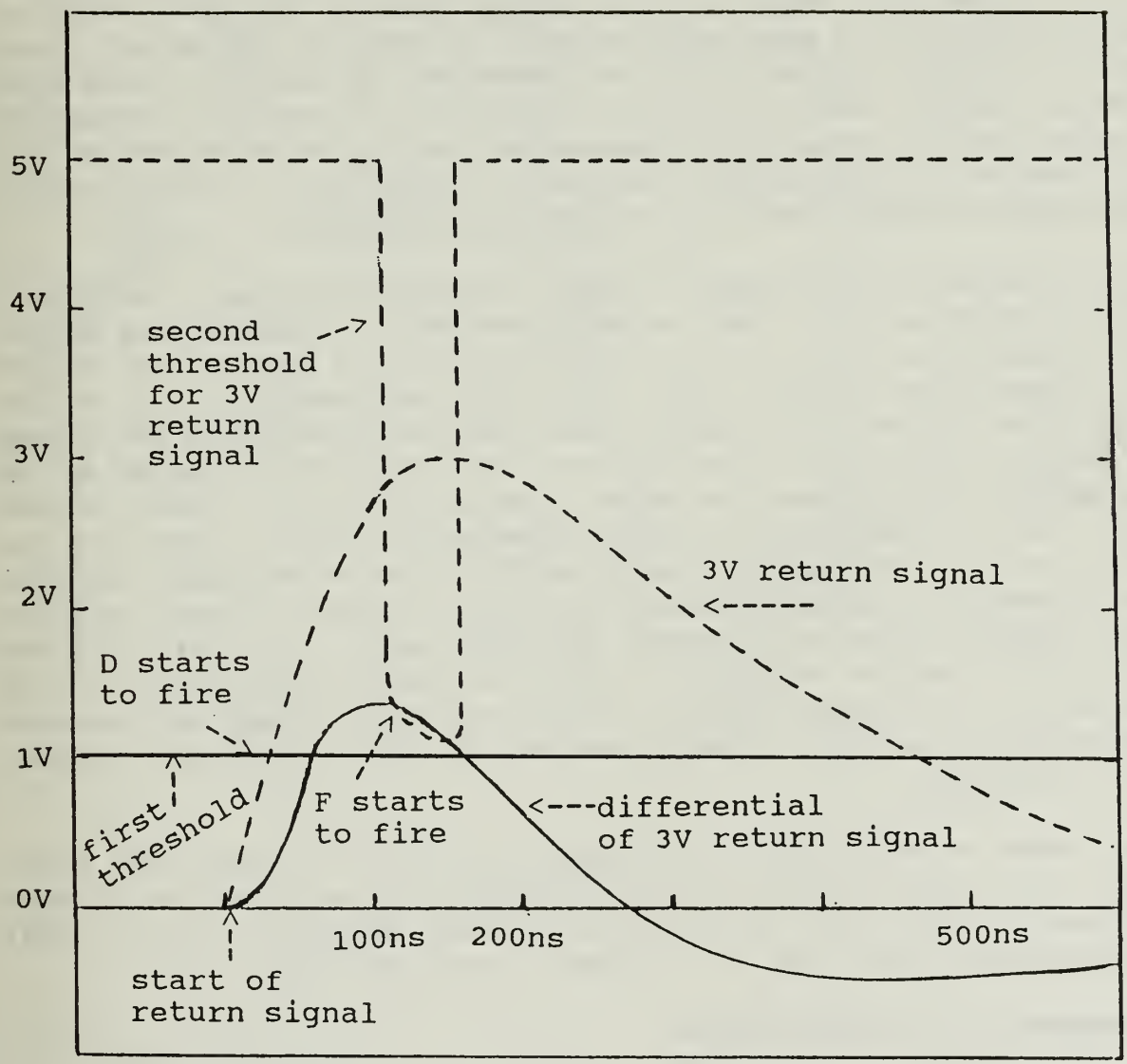

Figure 16. Trigger waveforms in improved leading edge circuit

6. Readout test pulser

The test pulser is a separate unit whose two outputs simulate those of the laser altimeter and which are fed into the altimeter readout. At this point we will simply state that the trigger output is practically identical to that of the laser altimeter. The leading edge of the signal output of the test pulser is a good approximation to that of the actual return signal. The signal output of the test pulser can be delayed in time using a helipot control. When it's control knob is set at zero, this corresponds to zero time for actual return signals out of the laser altimeter. The amplitude of the output pulse can also be varied up to 5 volts or more depending on the type of power supply used for the test pulser.

Fig. 17 is the circuit diagram of the readout test pulser. Internally mounted batteries allow either battery operation or ac operation by switching to one or the other. The 555 chip supplies the high to low trigger output pulse about 10 usec long. The 74121 chip supplies a high to low output about 3 usec in width whose exact width is controlled by the trimpot and helipot. The output is fed into the LM322 chip which triggers on the trailing edge of this input and yields a positive output pulse about 1 usec long. The 470 ohm, 33 pF network following it's output, slows down the leading edge to simulate the leading edge of the return signal from the laser altimeter. A variable voltage to LM322 (which is derived from the LM317 regulator) results in a variable amplitude output. The 2N4416 FET and the 2N2369 transistor form a driver which is capacitively coupled to the 50 ohm load in the altimeter readout. The output switch allows for a grounded output; this is used for a calibration step of the readout. See the section on Calibration.

The trimpot is used to make the zero position of the helipot dial correspond to the return signal of the laser altimeter at zero altitude (or zero distance). This is done by operating the laser altimeter at short range (say 6 meters) and correcting for the elapsed travel time (40 ns).

7. Calibration of the readout circuit

It is assumed that the readout test pulser is properly adjusted and both of its outputs are connected to the altimeter readout.

a. Internal settings.

There is a removable lid on the top of the readout package. Beneath it are the trace connections of the printed circuit board and three trimpots, hence the term internal settings. The first is the "initial voltage adjust", which is used to set the waveform at D2 to a lower level of 1.0 volt-this is the 1 volt threshold referred to previously. Next is the "final time-width adjust" which is used to set the time width of the waveform at F2 to 50- ns. Then the "final voltage adjust" is used to set the lower level of the waveform at F2 at about 2.5 volt; more precisely this is

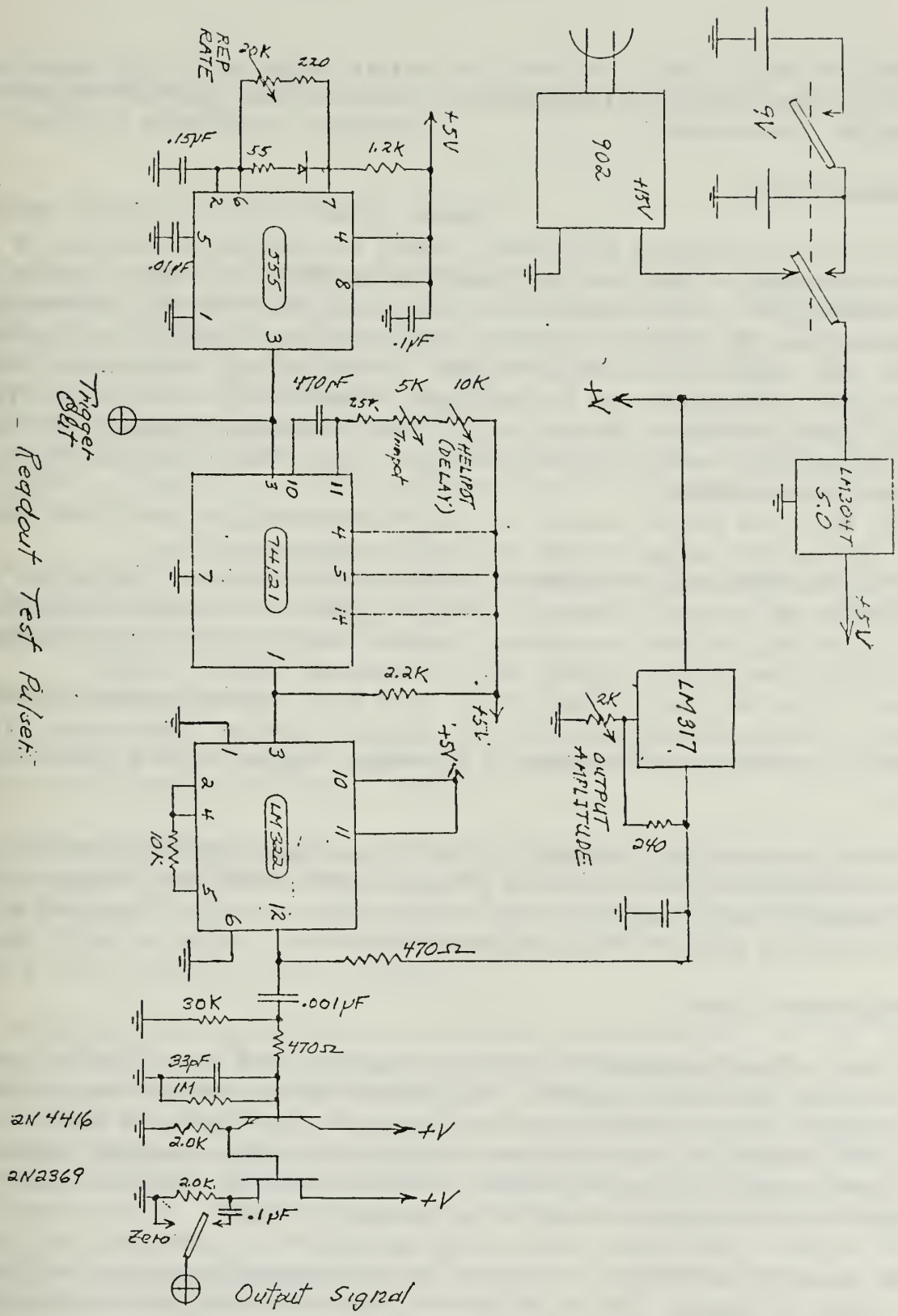

Figure 17. Readout test pulser

adjusted so that F just fires when the return signal is 3 volts amplitude. These are the nominal settings and once set are not part of the normal calibration of the readout.

b. External settings

There are three external adjustments which are located on the top of the readout package. These are the "zero time adjust", the "slope adjust" and the "bias adjust". The latter two have to do with the instrumentation amplifier (chip N), and the first one sets the time beginning of the ramp input. The following is the procedure for calibrating the readout, using the readout test pulser and an oscilloscope accurately calibrated in time. Also a digital voltmeter is connected to the "Altimeter Readout" BNC output. A constant test pulser output signal of 4.0 volts amplitude is normally used in what follows.

a. With the output switch of the readout test pulser (RTP) set to zero, regulate "Bias Adjust" so that the digital voltmeter reads zero.

b. Now with the output switch of RTP turned on and the helipot dial of the RTP set to zero, observe the output signal on the scope. Next move the helipot dial so that the signal advances exactly 160 ns (corresponds to 24 meters). Move the "zero adjust" until the voltmeter reads 0.48 volts.

c. Move the helipot dial of the RTP until the signal has advanced exactly 1 usec (150 meters) from it's original position. Now move "slope adjust" until the voltmeter reads 3.00 volts. Repeat steps b and c for a check.

The above procedure has been used where the maximum range measured has been under 150 meters. Obviously if a larger range is used, then in step c. the time delay is made exactly 2 usec (300 meters) and the "slope adjust" is moved to yield a 6.00 volt output on the voltmeter.

c. Temperature effects

The "zero adjust" essentially delays the start of the ramp relative to the start of the altimeter trigger. In the laser altimeter the laser is fired by a trigger which is also delayed (by about 3 usec) from the start of the altimeter trigger. So the timing accuracy of the readout assumes that when the "zero adjust" is properly made, that the start of the ramp waveform maintains a constant delay relative to the firing of the laser.

Temperature effects both in the laser altimeter and the readout may cause this delay to change. This is estimated to be the chief limit to accuracy of the readout due to temperature effects. In both these units the chips, resistances and capacitors involved are temperature dependent. The 74121 chip was purposely chosen for chip C because of its time stability. Actually the military version 54121 was used here; it has even better stability particularly for large temperature ranges. It is recommended that the military versions of all the chips used in the laser altimeter and altimeter readout be used whenever possible. The military version of chip N,

the instrumentation amplifier, should definitely be used, because of the two sensitive adjustments involved.

8. Power Supply for the Altimeter Readout

For lab tests and field tests near normal ac outlets an ac power source has been used for the power supply of the altimeter readout. The readout requires +5V, and V = 12V. The printed circuit is mounted as a unit onto a removable lid of a 7&1/4" x 10&1/4" aluminum box, 2&1/2" high. The bottom portion contains the power supply whose output is connected by a removable socket to the printed circuit on the lid. For the ac source, the +5V output of the AD923 DC power supply is used directly. The +/-15V outputs of the AD923 are fed to two 12V regulators i.e. the LM340t12 and 7912C to supply the +12V and -12V respectively.

For the battery operated power supply, a separate box bottom with nine Lithium batteries is substituted for the ac power source. Fig. A includes the circuitry and the pertinent data.

9. Dual Sequence Circuit

Fig. 15 first shows the basic schematic diagram of the two chips and then a sequence of illustrative trigger events.

As we have indicated in the Leading-Edge Detector section part (c), the return trigger inputs the dual sequence circuit. Whenever there are two return triggers in direct sequence, i.e. 1000 µsec apart, the dual sequence circuit gives an output, otherwise there is no output. See Fig. 10, chips O and P for a detailed circuit diagram.

The 74123 is a dual retriggerable monostable multivibrator. In Fig. 15(b) assume initially that both sections of the multivibrator are off. When the return trigger arrives, it fires the first section which stays on about 17 usec. After this the first section fires the second section which stays on for about 1250 µsec. The output of the second section inputs the 7432 chip which is an OR gate. Note this output is delayed by the 17 µsec period of the first section. The original return trigger also inputs the OR gate. Since B is high and A is low during the on time, the OR gate remains high. It will only go low when both A and B are low simultaneously; in other words it is a coincidence circuit.
Now we look further in time. The second return trigger, triggers the second half of 74123 which then goes low, but 1000 µsec after the second return trigger we have the third return trigger. This re-triggers the 74123 and keeps its final output low. Similarly for the fourth trigger. Therefore the third and fourth return triggers result in outputs from the OR gate.

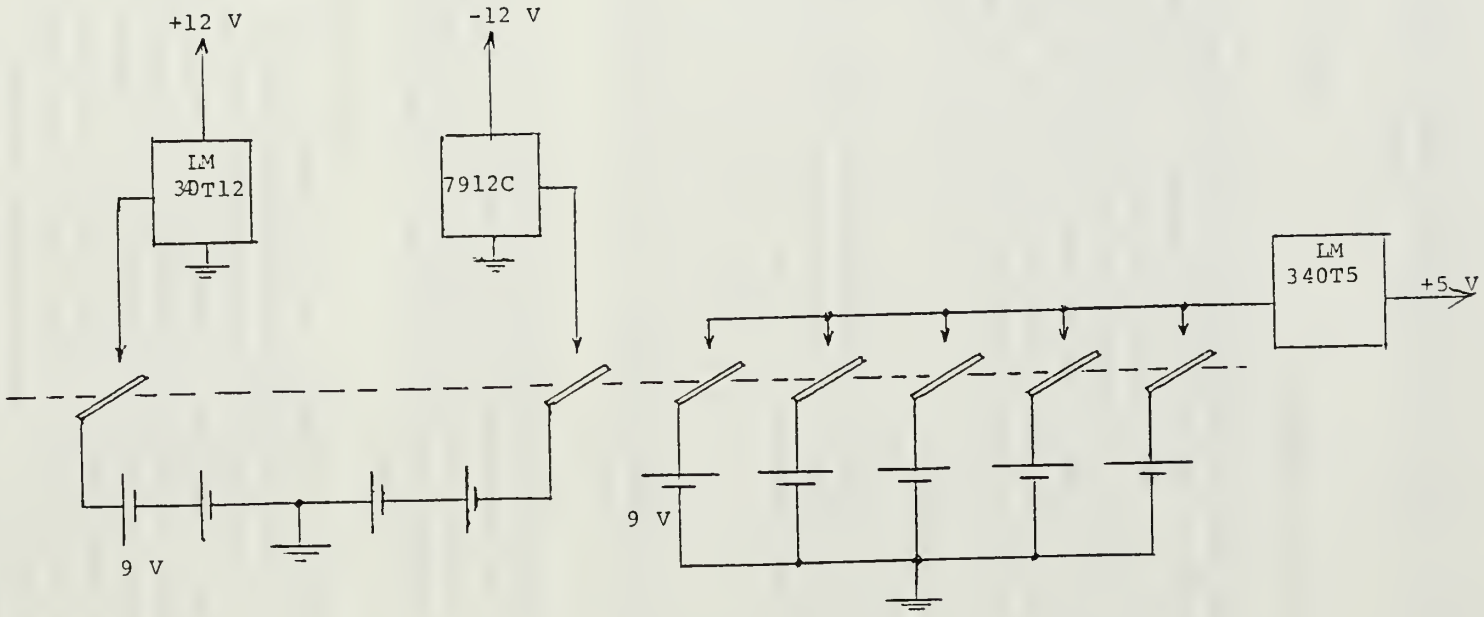

All nine batteries are 9 volt Duracell XL LD323A lithium batteries.

The current drain at +12 V is about 36 ma
at -12 V is about 22 ma
at + 5 V is about 164 ma.

At these current values the batteries should give about 30 hours of service according to the manufacturers specifications.

Figure 18. Power supply circuit

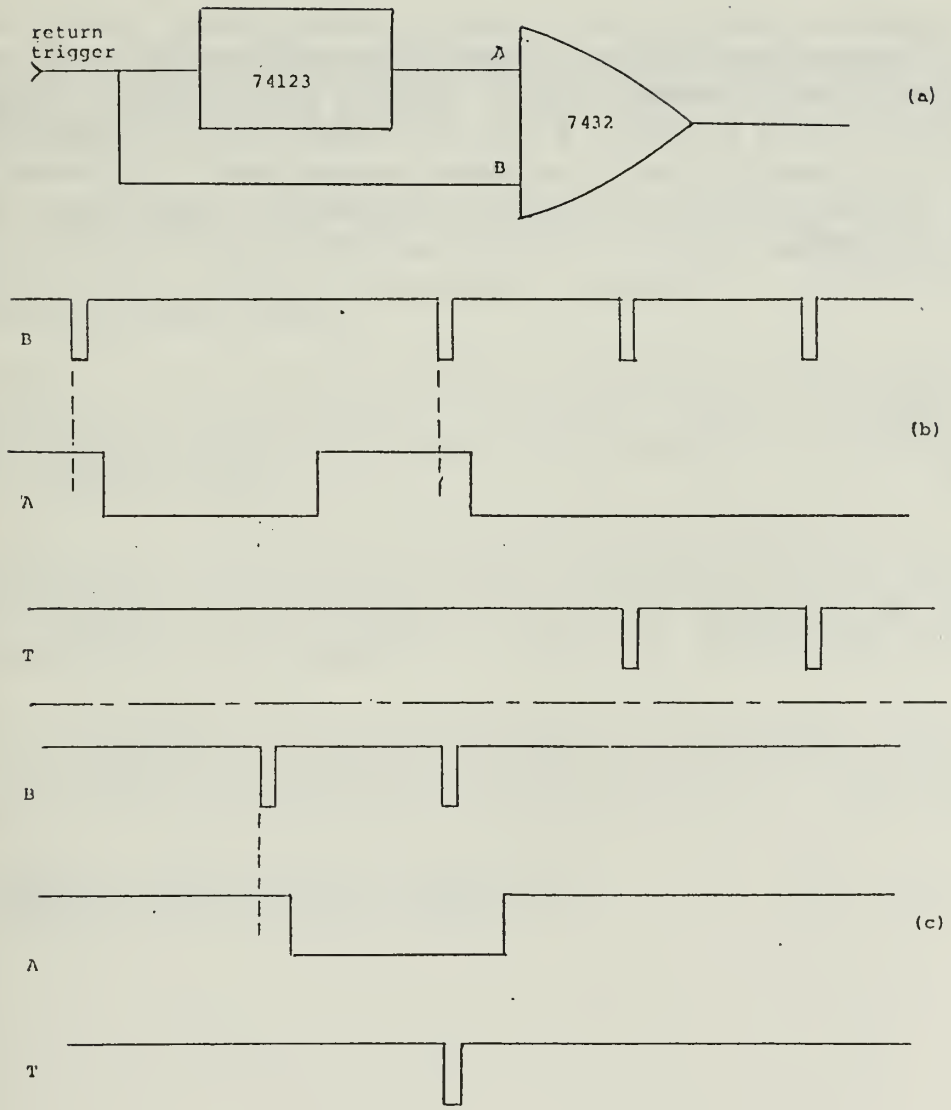

Figure 19. Dual sequence trigger

Fig. 19(c) is a further illustration of how the dual sequence trigger operates.

10. Cost Estimate

The most expensive items in the altimeter readout circuit are the Lithium batteries for the power supply. These now cost $11.55 each, totaling $103.95 for the nine unit battery pack. The next most expensive item is the AD521 instrumentation amplifier which was listed at about $42.00 several years ago. The remaining parts are fairly conventional chips,resistors and capacitors. So the total cost of parts is far below a target cost of $1000 that had been proposed.

LIST OF REFERENCES

1. Gilio, J. P., Initial Development of a Laser Altimeter, Master's Thesis, Naval Postgraduate School, September 1985.

2. Petri, K., "Laser Radar Reflectance of Chesapeake Bay Waters as a Function of Wind Speed," IEEE Transactions on Geoscience Electronics, V. 15, No. 2, pp 87-96, April 1977.

3. Cox, C. and Munk, W., "Measurement of the Roughness of the Sea Surface from Photographs of the Sun's Glitter," Journal of the Optical Society of America, V. 44, pp 838-850, November 1954.

4. Schooley, A., "A Simple Optical Method for Measuring the Statistical Distribution of Water Surface Slopes," Journal of the Optical Society of America, V. 44, pp 37-40, January 1954.

5. Swennen, J., "Time-Average Surface-Reflected Energy Received from a Collimated Beam of Radiant Energy Normally Incident on the Ocean Surface," Journal of the Optical Society of America, V. 58, pp. 47-51, January 1968.

6. Guinn, J., Plass, G., and Kattawar, G. "Sunlight Glitter on a Wind-Ruffled Sea: Further Studies," Applied Optics, V. 18, pp 842-849, 15 March 1959.

7. 468 Digital Storage Oscilloscope, V. 1, Tektronix, Inc., Beaverton, Oregon, 1981.

DISTRIBUTION LIST

1.	Defense Technical Information Center Cameron Station Alexandria, VA 22304-6145	2
2.	Library, Code 1042 Naval Postgraduate School Monterey, CA 93943-5002	2
3.	Professor K. E. Woehler, Code 61Wh Chairman, Department of Physics Naval Postgraduate School Monterey, CA 93943-5000	2
4.	Professor E. C. Crittenden, Jr. Department of Physics Naval Postgraduate School Monterey, CA 93943-5000	2
5.	Professor A. W. Cooper Department of Physics Naval Postgraduate School Monterey, CA 93943-5000	20
6.	Professor G. W. Rodeback Department of Physics Naval Postgraduate School Monterey, CA 93943-5000	2
7.	LCDR Carlton M. Bourne Naval Sea Systems Command Headquarters (PMS-405) Washington, DC 20362-5101	1
8.	Commander, Naval Sea Systems Command ATTN: SEA 06-W31 (C. Espeland) Washington, DC 20362-5101	2
9.	Commander, Naval Sea Systems Command ATTN: PMS 421 CAPT J. Paine Washington, DC 20362-5101	1
10.	Commander, Space and Naval Warfare Systems Command ATTN: PMW 145 (M. Madden and E. Turner) Washington, DC 20362-5101	2
11.	Commander, Pacific Missile Test Center ATTN: Code 4030 (R. Mark) Point Mugu, CA 93042-5000	1
12.	U. S. Coast Guard R & D Center ATTN: Frank S. Replogle, Jr. Avery Point, Groton, CT 06340	1

13. Commander, Naval Environmental Prediction Research Facility 1
ATTN: J. Cook
Naval Warfare Support Department
Monterey, CA 93943-5006

14. Commander, Naval Environmental Prediction Research Facility 1
ATTN: M. Sierchio
Naval Warfare Support Department
Monterey, CA 93943-5006

15. The Johns Hopkins University 1
Applied Physics Laboratory
ATTN: Dr. R. Steinberg
Johns Hopkins Road
Laurel, MD 20707

16. Georgia Tech Research Institute 1
Georgia Institute of Technology
ATTN: K. R. Johnson
Electromagnetics Laboratory
Atlanta, GA 30322

17. Grumman Corporate Research Center 1
ATTN: Dr. J. Krassner
Optical Physics
Bethpage, NY 11714-3580

18. Director, Research Administration, Code 012 1
Naval Postgraduate School
Monterey, CA 93943